SUPPORTING INFORMATION

Volatile Lanthanide Complexes with Fluorinated Heptadentate Ligands

Joshua C. Zgrabik,[1] Balaka Bhuniya,[1] Thomas Branstad Phillips,[1] Jorge Barroso,[2] Bess Vlaisavljevich,[2] and Scott R. Daly[1]*

[1]Department of Chemistry, The University of Iowa, E331 Chemistry Building, Iowa City, Iowa 52242, United States.

[2]Department of Chemistry, The University of South Dakota, 414 E Clark St., Vermillion SD, 57069, United States.

Corresponding Email: scott-daly@uiowa.edu

Table of Contents

I. Crystallographic data

Table S1. Crystallographic data collected at 150(1) K for **Yb-1** (R, R′ = CF_3), **Yb-2** (R = $CF_2CF_2CF_3$, R′ = CF_3), **Yb-4** (R = CF_3, R′ = Me), **Er-1** (R, R′ = CF_3), and **Nd-3** (R = $CF_2CF_2CF_3$, R′ = ^{t}Bu).

	Yb-1	**Yb-2**	**Yb-4**	**Er-1**	**Nd-3**
Formula	$C_{21}H_{15}F_{18}N_4O_3Yb$	$C_{27}H_{15}F_{30}N_4O_3Yb$	$C_{21}H_{24}F_9N_4O_3Yb$	$C_{21}H_{15}ErF_{18}N_4O_3$	$C_{36}H_{42}F_{21}N_4NdO_3$
Identifier	dal2071	dal2127	dal2161	dal219	dal2120
FW (g mol^{-1})	886.41	1186.47	798.60	880.63	1121.97
crystal system	Monoclinic	Triclinic	Orthorhombic	Triclinic	Triclinic
space group	$P2_1/c$	P-1	$Pbca$	P-1	P-1
a (Å)	18.1775(18)	10.0912(10)	19.7260(19)	8.1560(8)	7.2329(7)
b (Å)	10.2981(10)	10.4385(10)	19.9703(19)	14.0106(14)	14.5721(15)
c (Å)	17.0455(17)	17.6508(18)	15.5564(15)	14.8598(15)	21.231(2)
α (deg)	90	89.530(5)	90	117.742(5)	92.033(5)
β (deg)	116.043(5)	86.742(5)	90	93.538(5)	90.548(5)
γ (deg)	90	86.666(5)	90	91.261(5)	92.205(5)
volume (Å)^3	2866.8(5)	1853.1(3)	6128.2(10)	1497.5(3)	2234.5(4)
Z	4	2	8	2	2
ρ_{calc} (g cm^{-3})	2.054	2.126	1.731	1.953	1.668
μ (mm^{-1})	3.412	2.713	3.144	2.945	1.289
F (000)	1700	1138	3160	846	1118
θ range (deg)	25.242	25.242	25.242	25.242	25.242
R (int)	0.0827	0.0247	0.0474	0.0327	0.0380
data/restraints/parameters	5785/0/425	7590/36/638	6289/0/393	6126/0/424	10552/0/595
GOF	1.028	1.096	1.186	1.068	1.066
R_1 [$I > 2\sigma(I)$][a]	0.0372	0.0267	0.0379	0.0241	0.0275
wR_2 (all data)[b]	0.0755	0.0682	0.0881	0.0605	0.0616
Largest Peak/Hole (e · Å^{-3})	0.880/-1.393	1.596/-0.502	1.434/-2.355	1.290/-0.695	0.515/-0.683

[a] $R_1 = \Sigma\, |F_o| - |F_c| \,| / |\Sigma|F_o|$ for reflections with $F_o^2 > 2\sigma(F_o^2)$.

[b] $wR_2 = [\Sigma w(F_o^2 - F_c^2)^2 / \Sigma(F_o^2)^2]^{1/2}$ for all reflections.

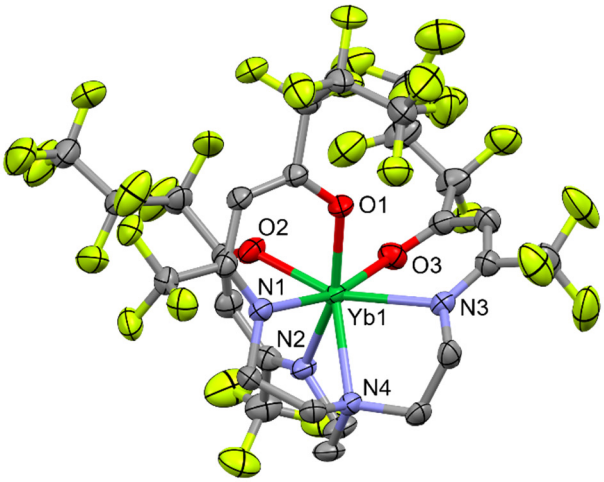

Figure S1. Molecular structure of **Yb-2** (R = $CF_2CF_2CF_3$, R′ = CF_3) with thermal ellipsoids at 50% probability. Hydrogen atoms are omitted from the figure.

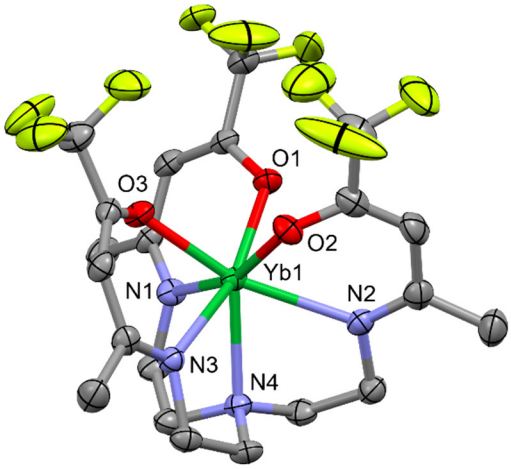

Figure S2. Molecular structure of **Yb-4** (R = CF_3, R′ = Me) with thermal ellipsoids at 50% probability. Hydrogen atoms are omitted from the figure.

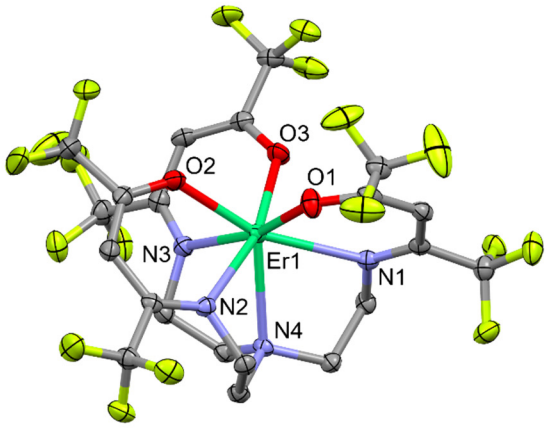

Figure S3. Molecular structure of **Er-1** (R, R′ = CF_3) with thermal ellipsoids at 50% probability. Hydrogen atoms are omitted from the figure.

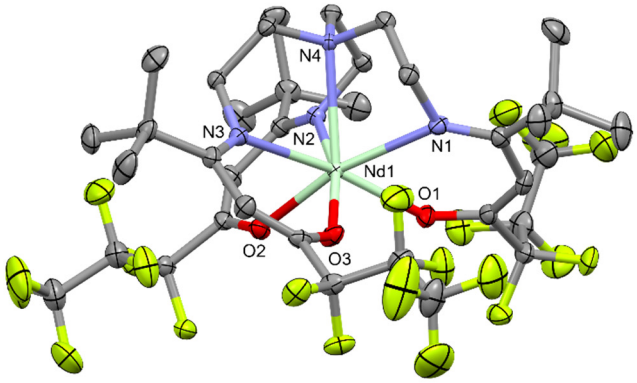

Figure S4. Molecular structure of **Nd-3** (R = $CF_2CF_2CF_3$, R′ = ^{t}Bu) with thermal ellipsoids at 50% probability. Hydrogen atoms are omitted from the figure.

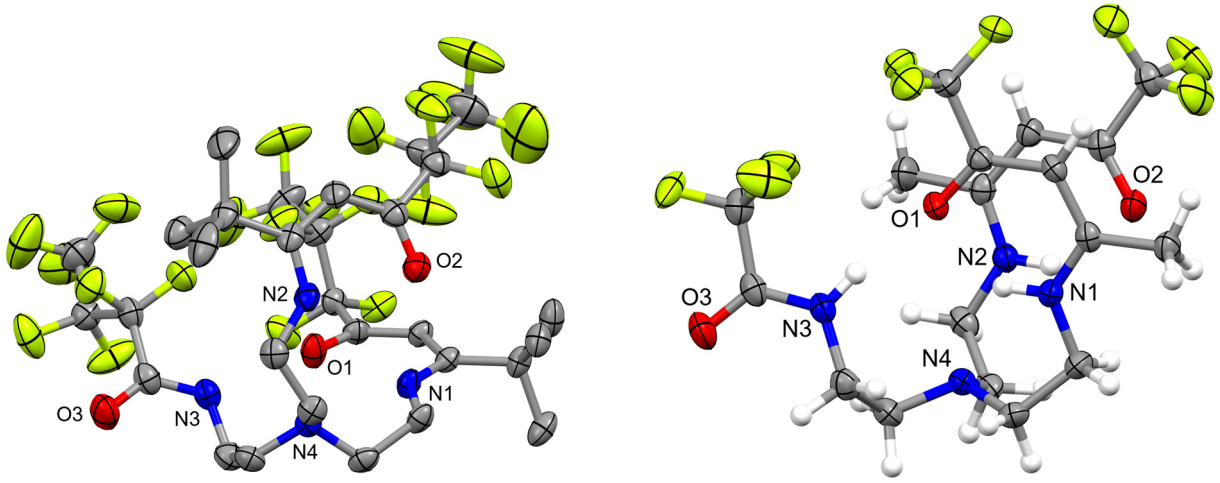

Figure S5. Molecular structures of monoamide side products isolated from attempted synthesis of H_3(**3**) (left; hydrogens not shown) and H_3(**4**) (right) under certain conditions. Thermal ellipsoids at 50% probability. The amide arms contain the atoms labeled N3 and O3. Disordered C-F components were omitted from the figure.

II. NMR spectra

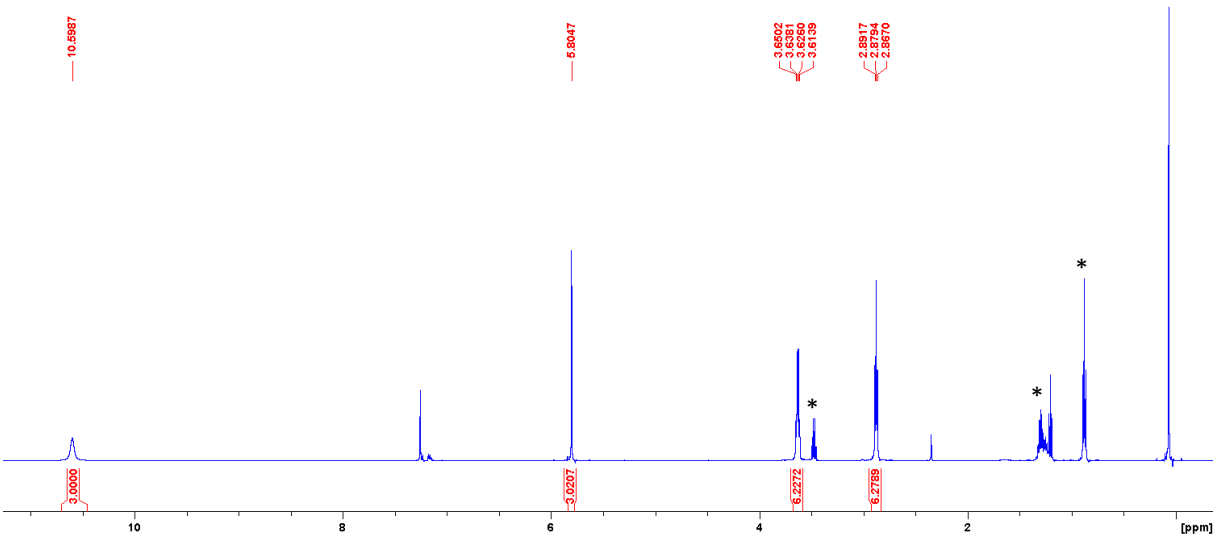

Figure S6. ^{1}H NMR spectrum of CF_3TRAC, H_3(**1**), in $CDCl_3$. The * symbol indicates resonances assigned to residual pentane and Et_2O.

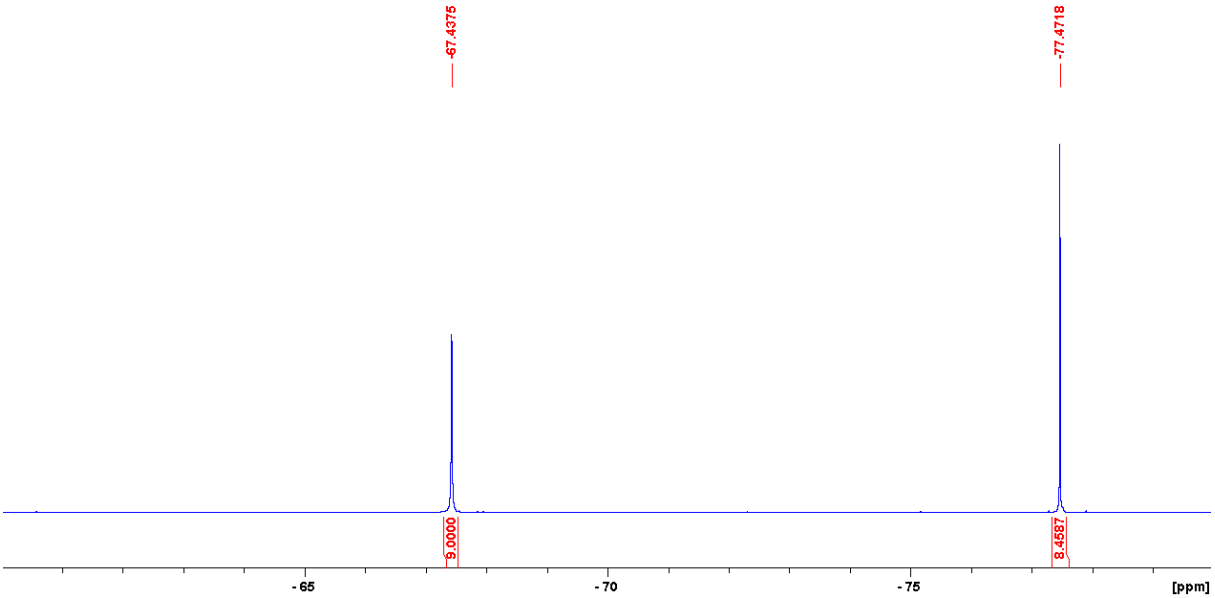

Figure S7. ^{19}F NMR spectrum of CF_3TRAC, H_3(**1**), in $CDCl_3$.

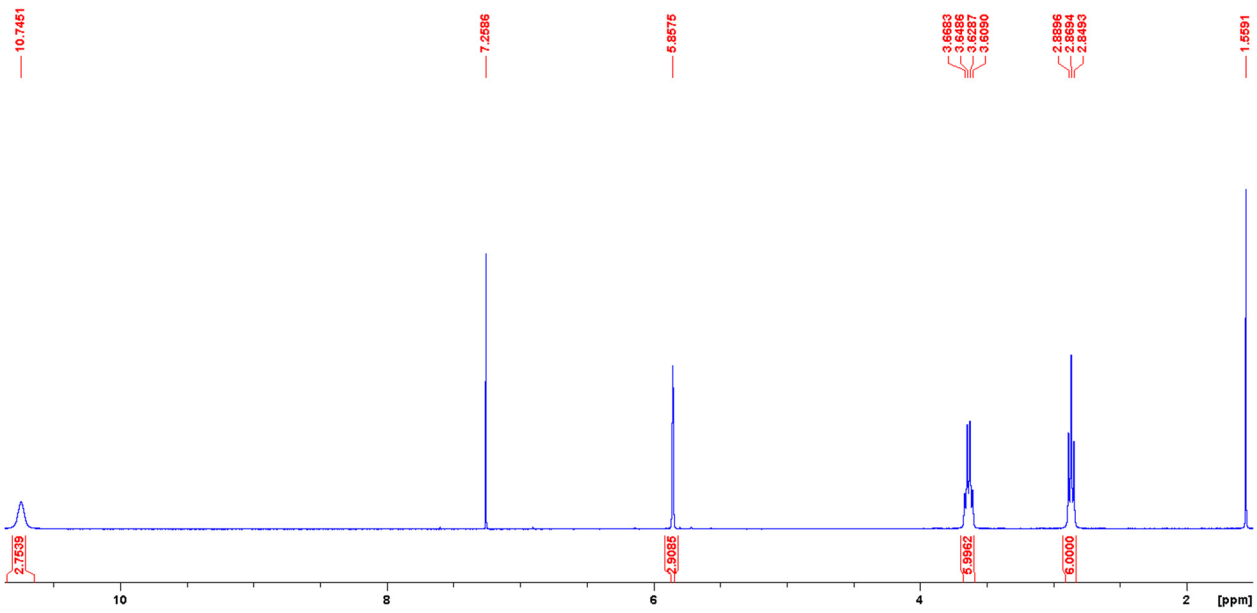

Figure S8. ^{1}H NMR spectrum of $CF_3C_3F_7$TRAC, H_3(**2**), in $CDCl_3$.

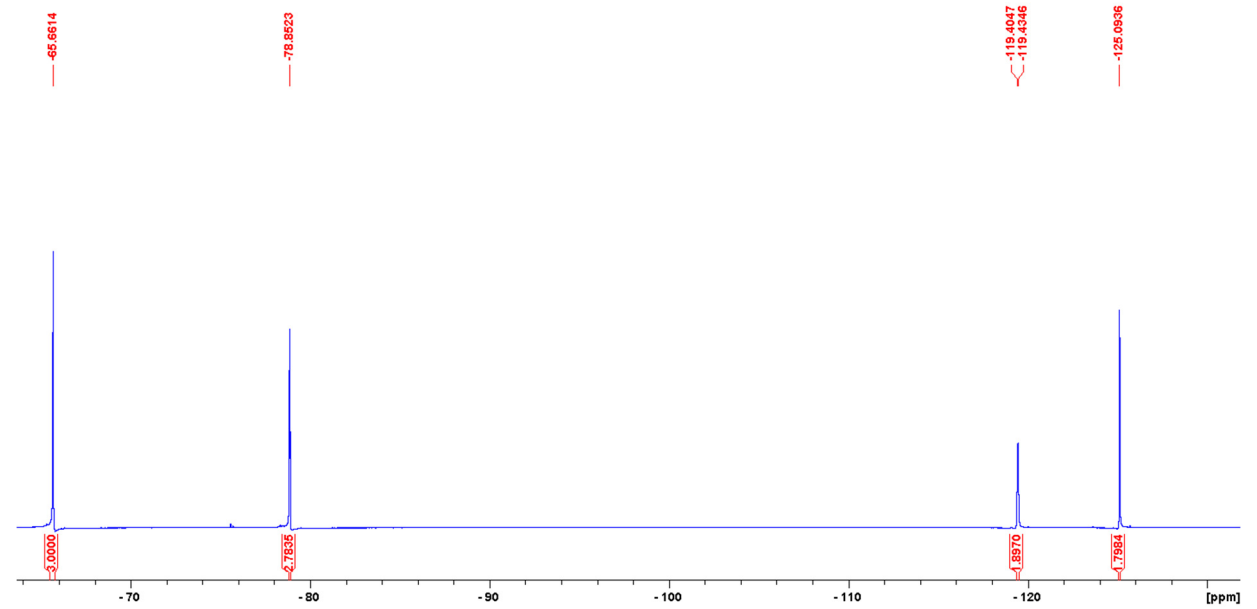

Figure S9. ^{19}F NMR spectrum of $CF_3C_3F_7$TRAC, H_3(**2**), in $CDCl_3$.

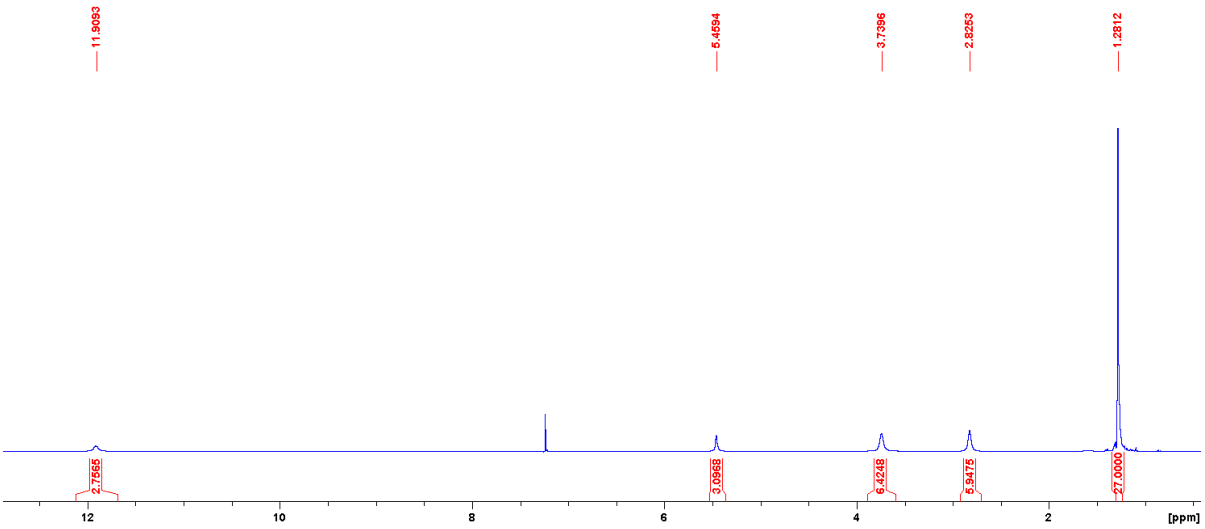

Figure S10. ^{1}H NMR spectrum of ^{t}BuC$_3$F$_7$TRAC, H$_3$(**3**), in CDCl$_3$.

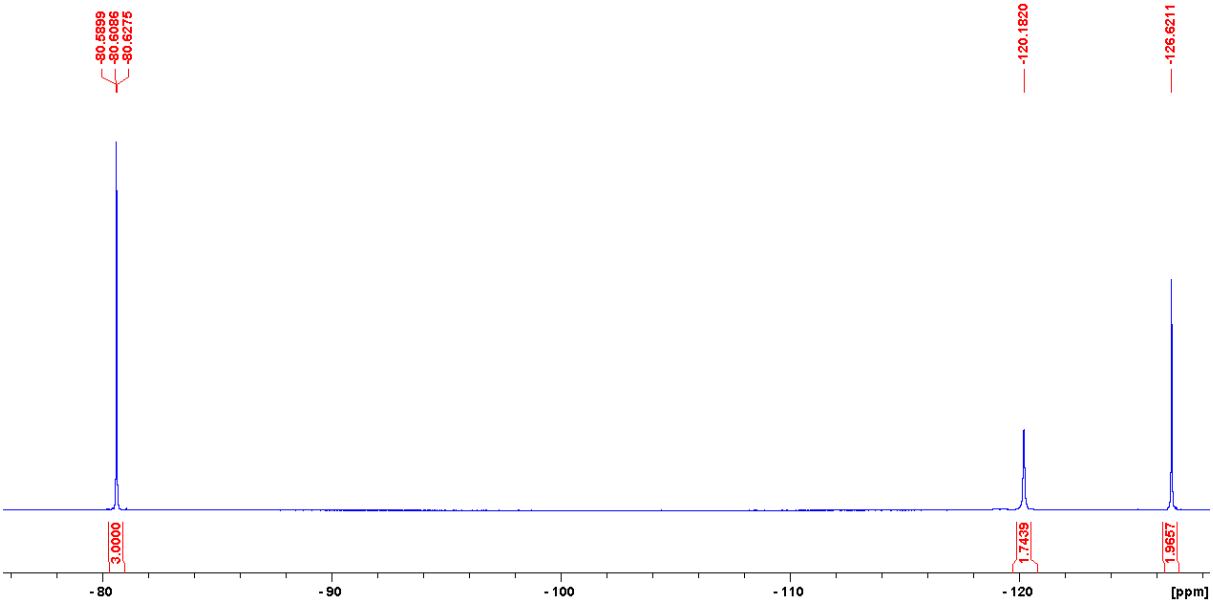

Figure S11. ^{19}F NMR spectrum of ^{t}BuC$_3$F$_7$TRAC, H$_3$(**3**), in CDCl$_3$.

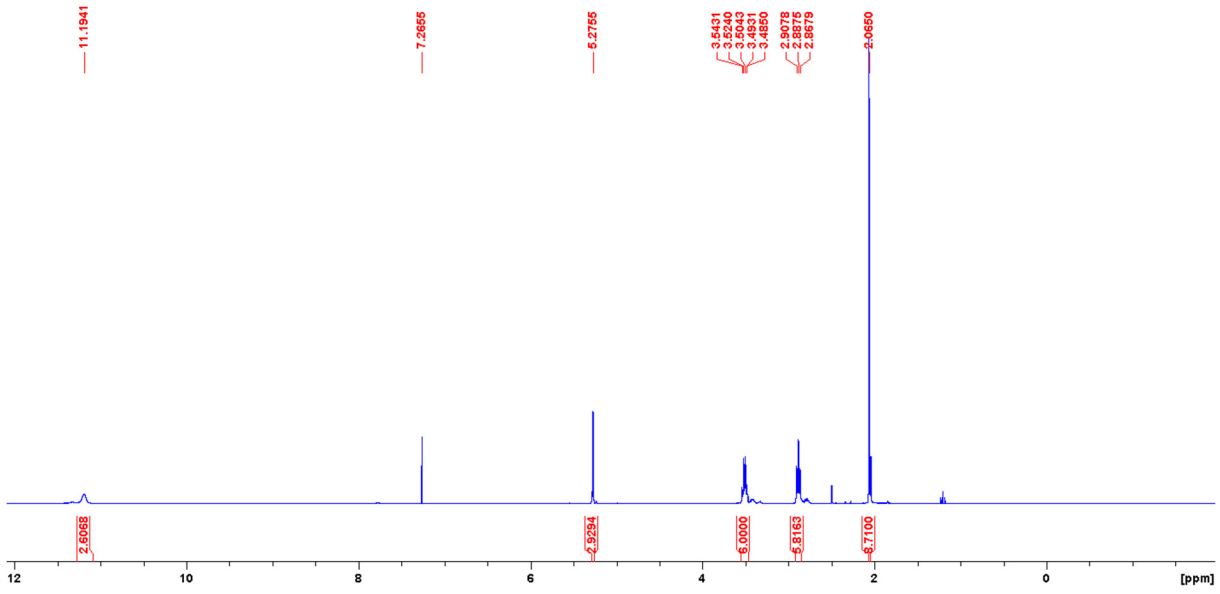

Figure S12. ^{1}H NMR spectrum of $MeCF_3TRAC$, H_3(**4**), in $CDCl_3$.

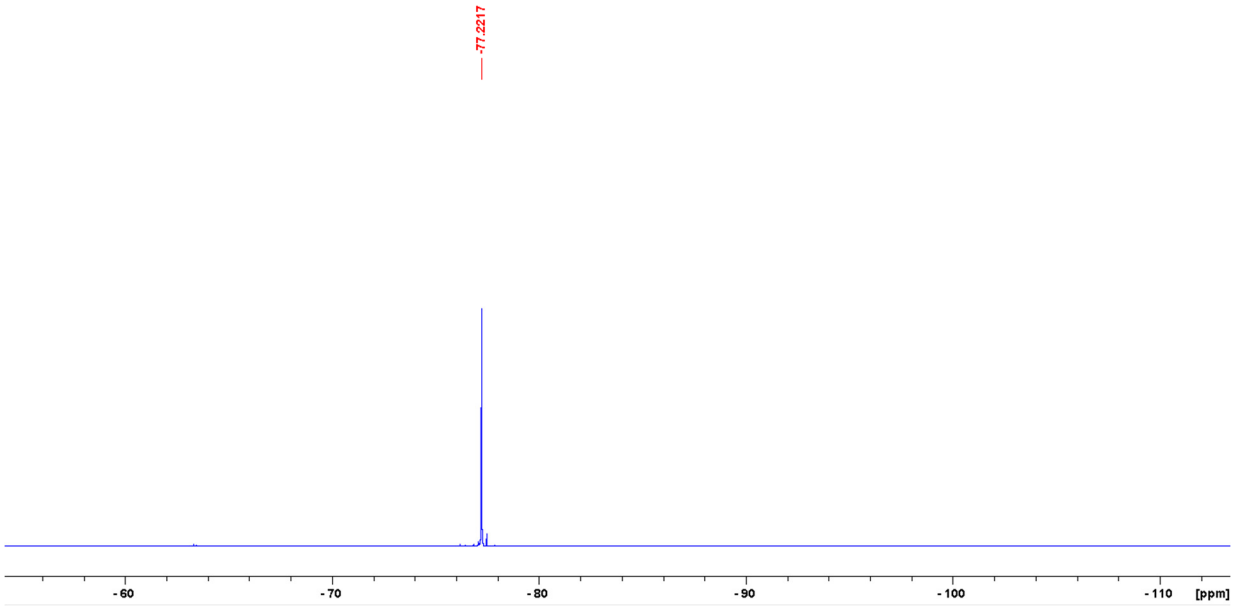

Figure S13. ^{19}F NMR spectrum of $MeCF_3TRAC$, H_3(**4**), in $CDCl_3$.

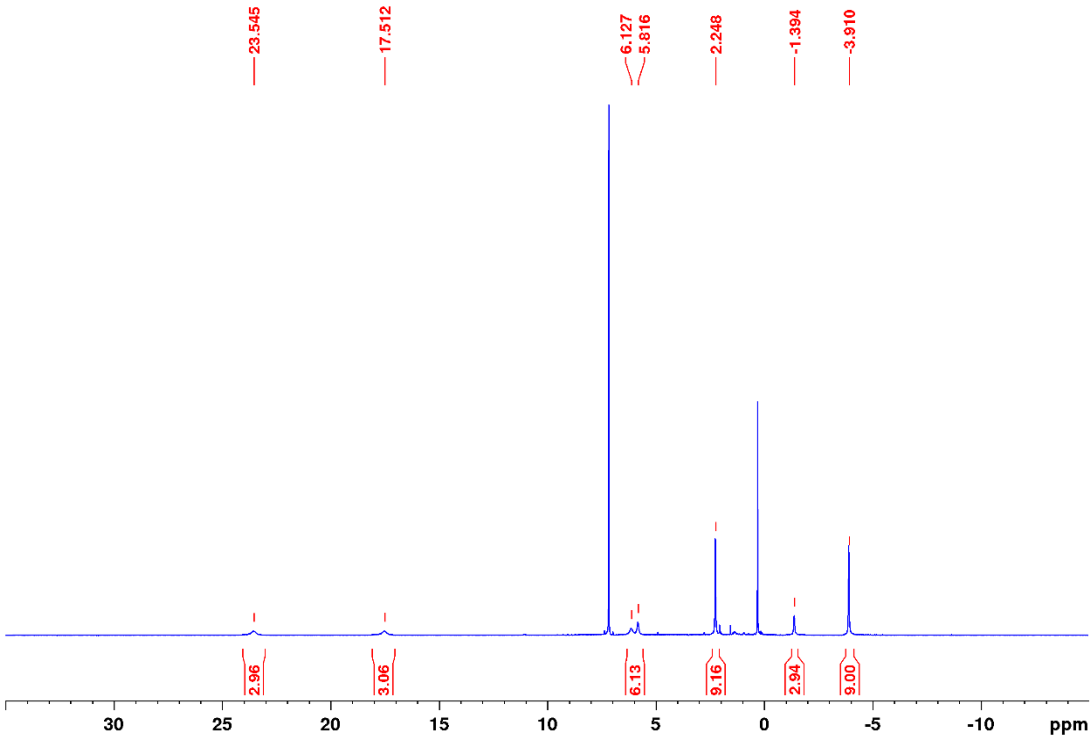

Figure S14. ^{1}H NMR spectrum of **Yb(TRAC)** in C_6D_6.

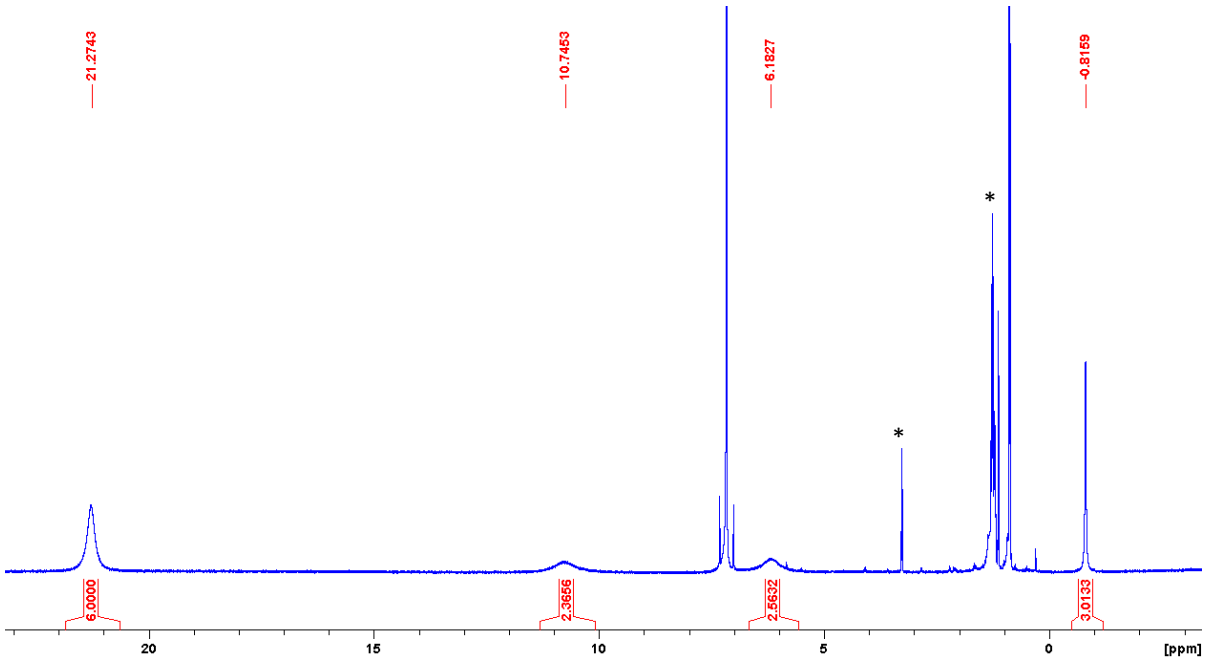

Figure S15. ^{1}H NMR spectrum of **Yb-1** (R, R′ = CF_3) in C_6D_6. The * symbol indicates resonances assigned to residual pentane and diethyl ether.

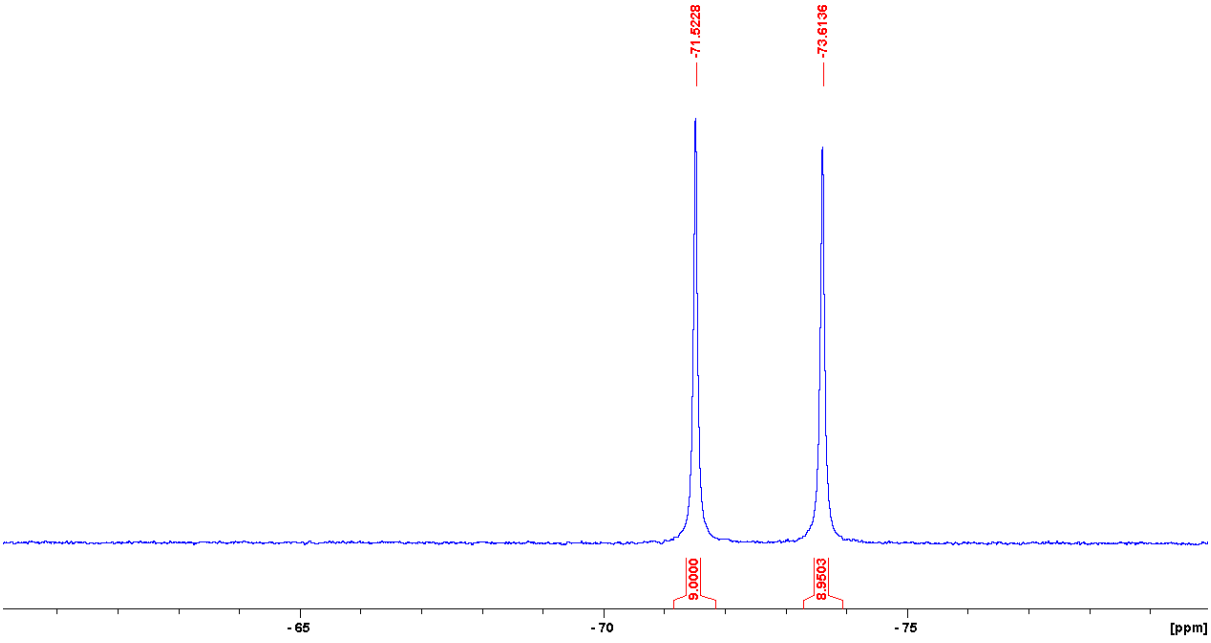

Figure S16. ^{19}F NMR spectrum of **Yb-1** (R, R′ = CF_3) in C_6D_6.

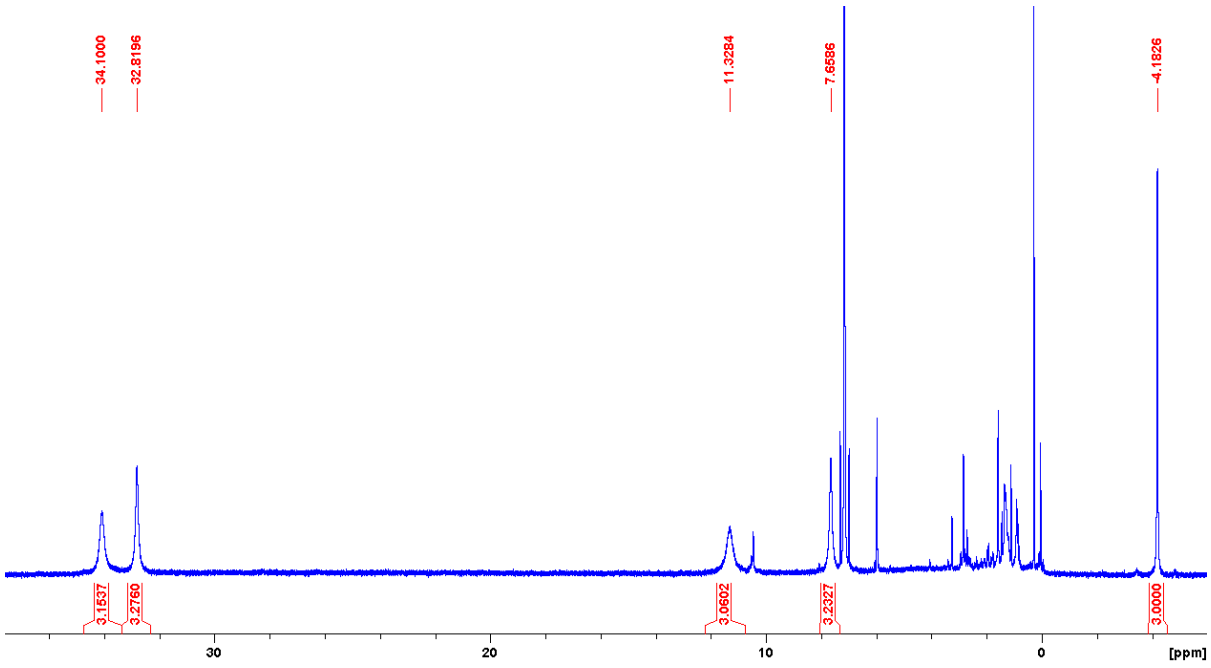

Figure S17. ^{1}H NMR spectrum of **Yb-2** (R = $CF_2CF_2CF_3$, R′ = CF_3) in C_6D_6. Unlabeled resonances are assigned to unreacted ligand, Et_2O, pentane, and grease.

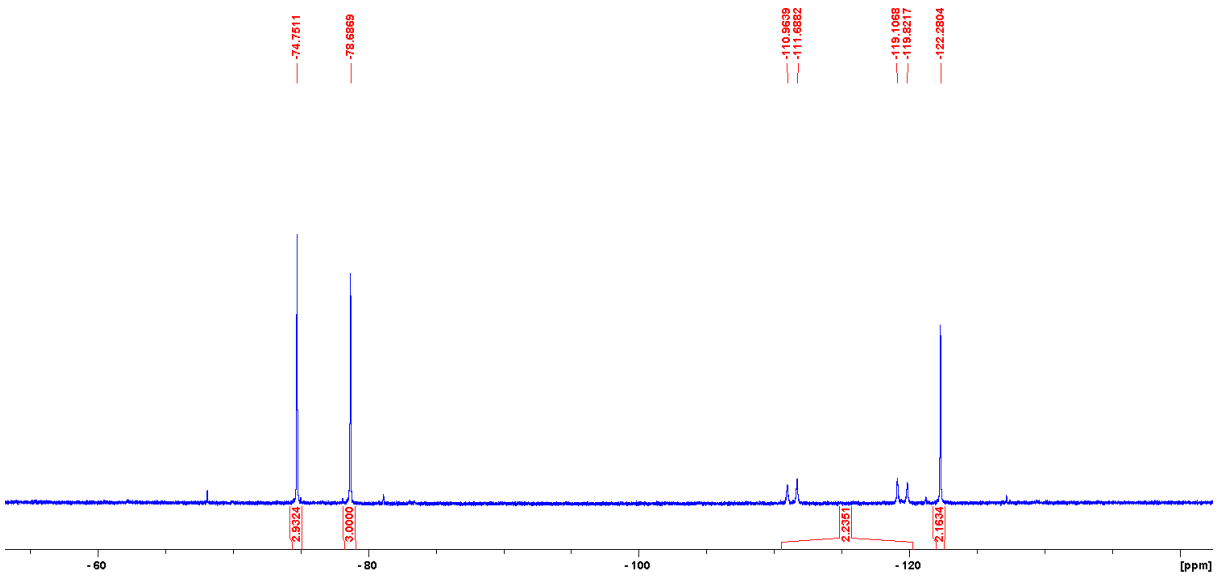

Figure S18. ^{19}F NMR spectrum of **Yb-2** (R = $CF_2CF_2CF_3$, R′ = CF_3) in C_6D_6.

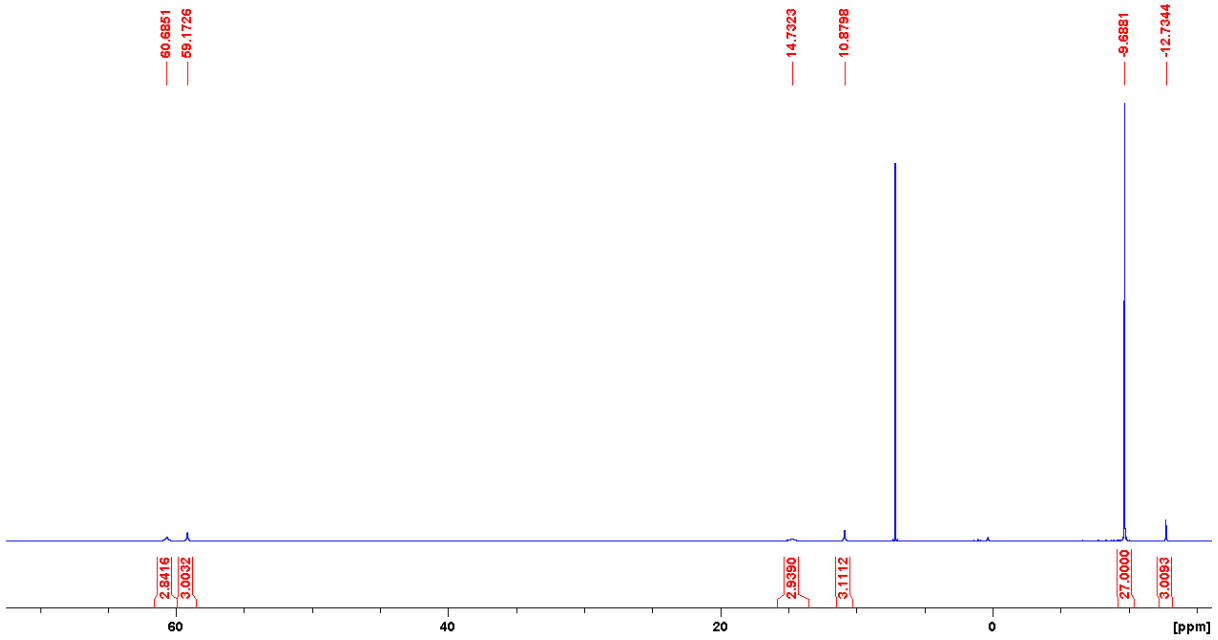

Figure S19. ^{1}H NMR spectrum of **Yb-3** (R = $CF_2CF_2CF_3$, R′ = ^{t}Bu) in C_6D_6.

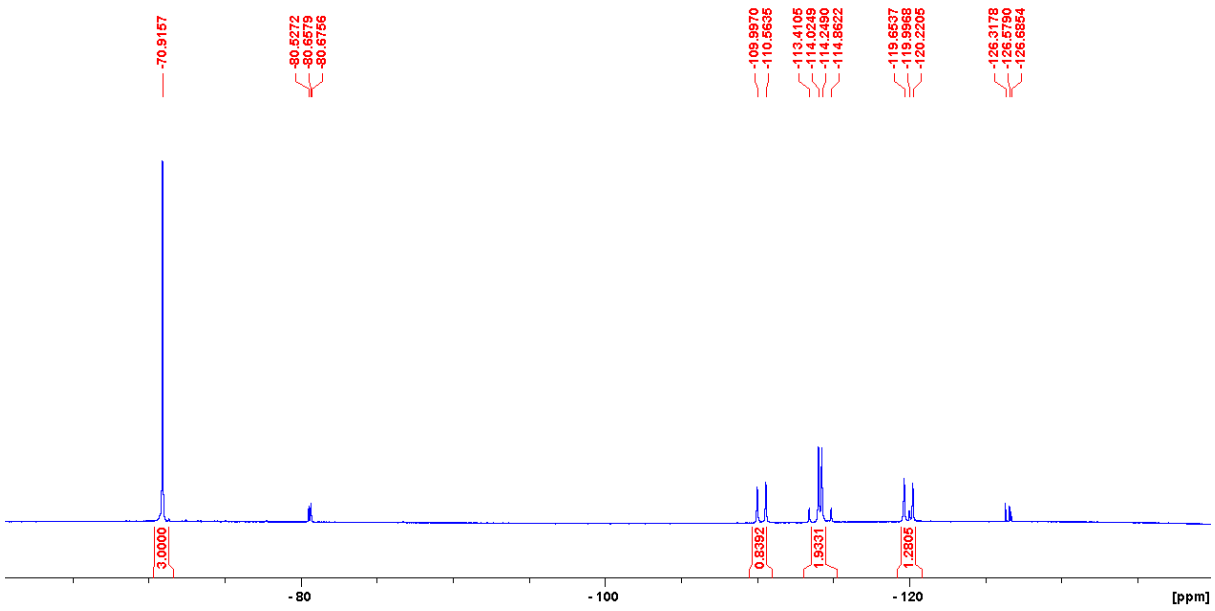

Figure S20. ^{19}F NMR spectrum of **Yb-3** (R = $CF_2CF_2CF_3$, R′ = ^{t}Bu) in C_6D_6.

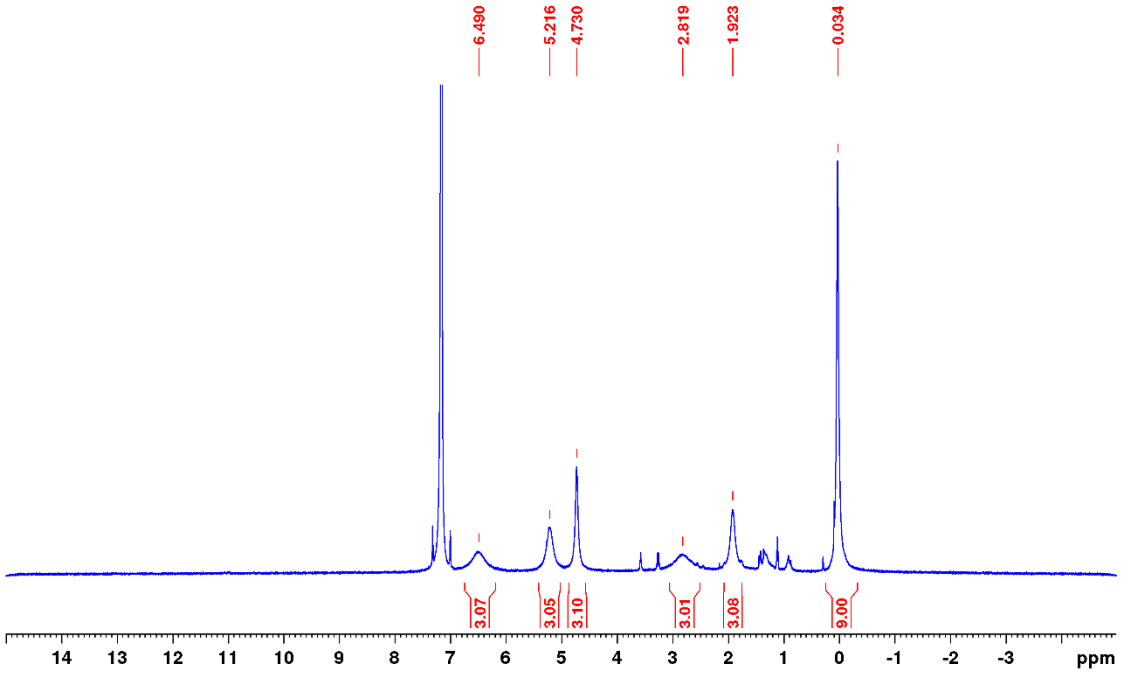

Figure S21. ^1H NMR spectrum of **Yb-4** (R = CF_3, R′ = Me) in C_6D_6.

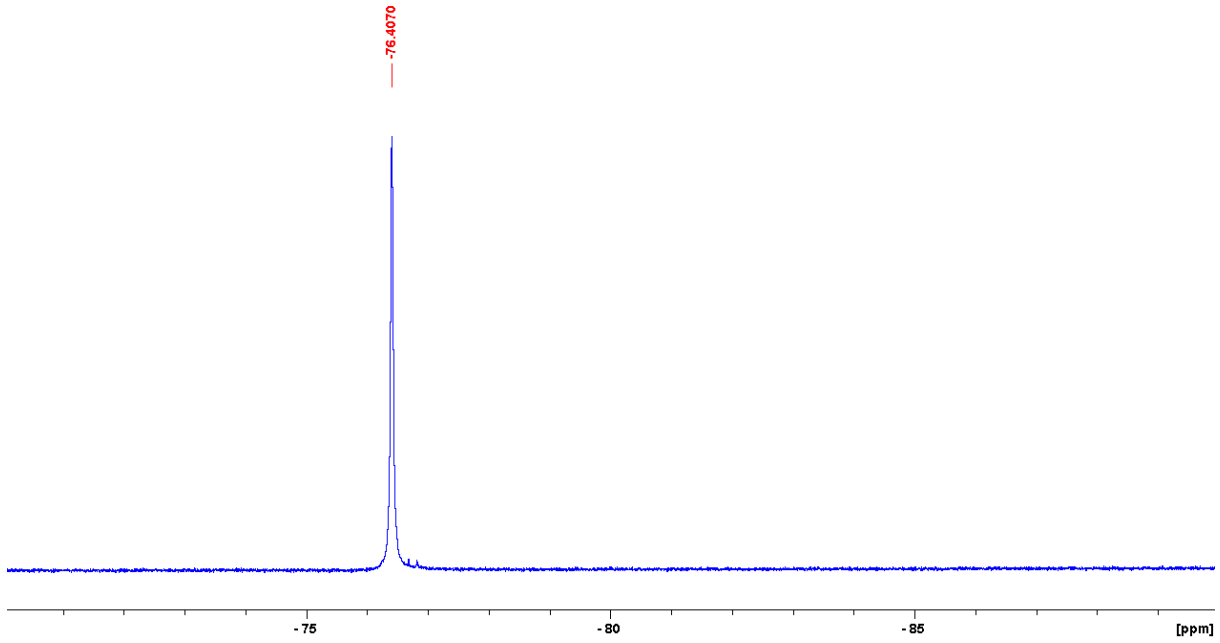

Figure S22. ^{19}F NMR spectrum of **Yb-4** (R = CF_3, R′ = Me) in C_6D_6.

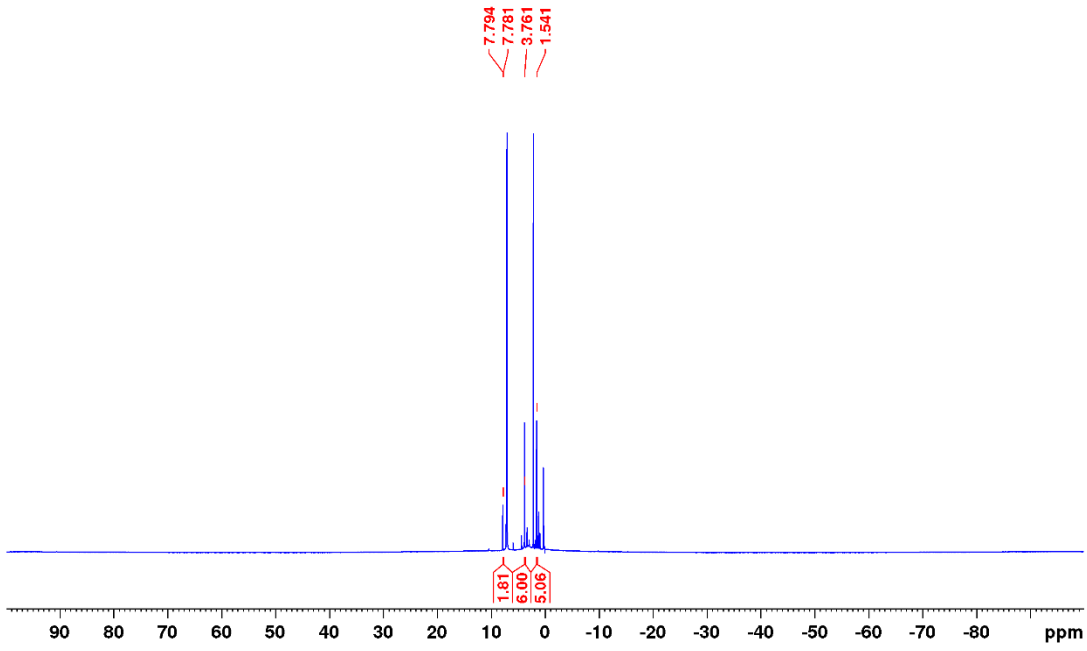

Figure S23. ^1H NMR spectrum of **Er-1** (R, R′ = CF_3) in C_7D_8. Only diamagnetic resonances associated with residual solvent, grease, and H_3(**1**) were observed in the spectral window shown.

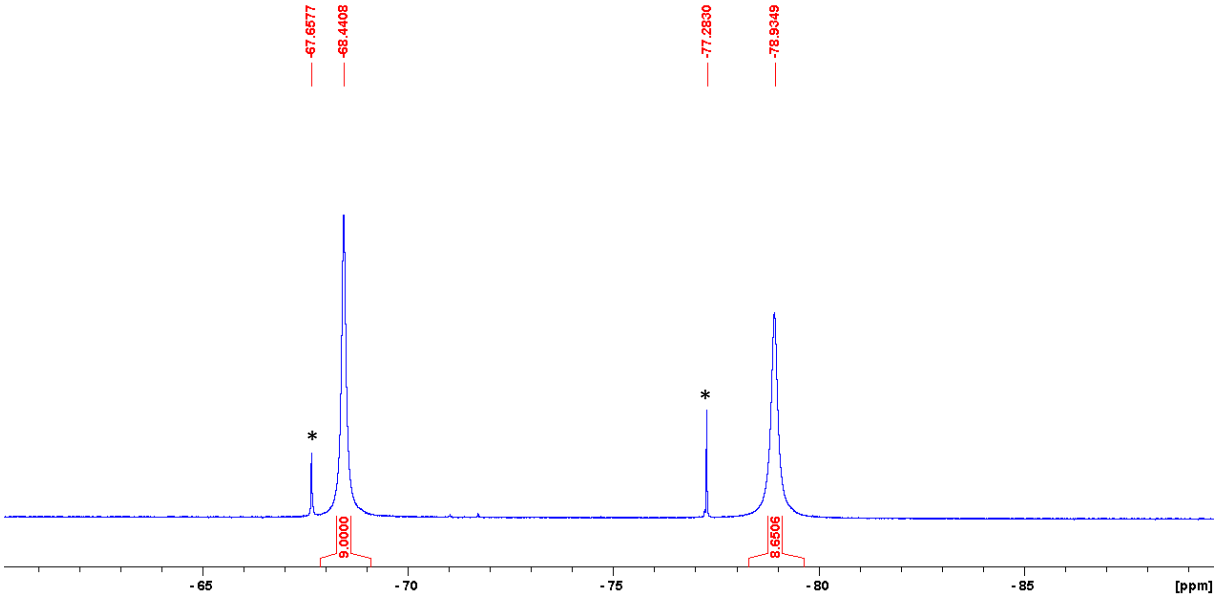

Figure S24. ^{19}F NMR spectrum of **Er-1** (R, R′ = CF_3) in C_7D_8. The * symbol indicates resonances assigned to H_3(**1**) ligand (ca. 5% by integration compared to resonances for **Er-1**).

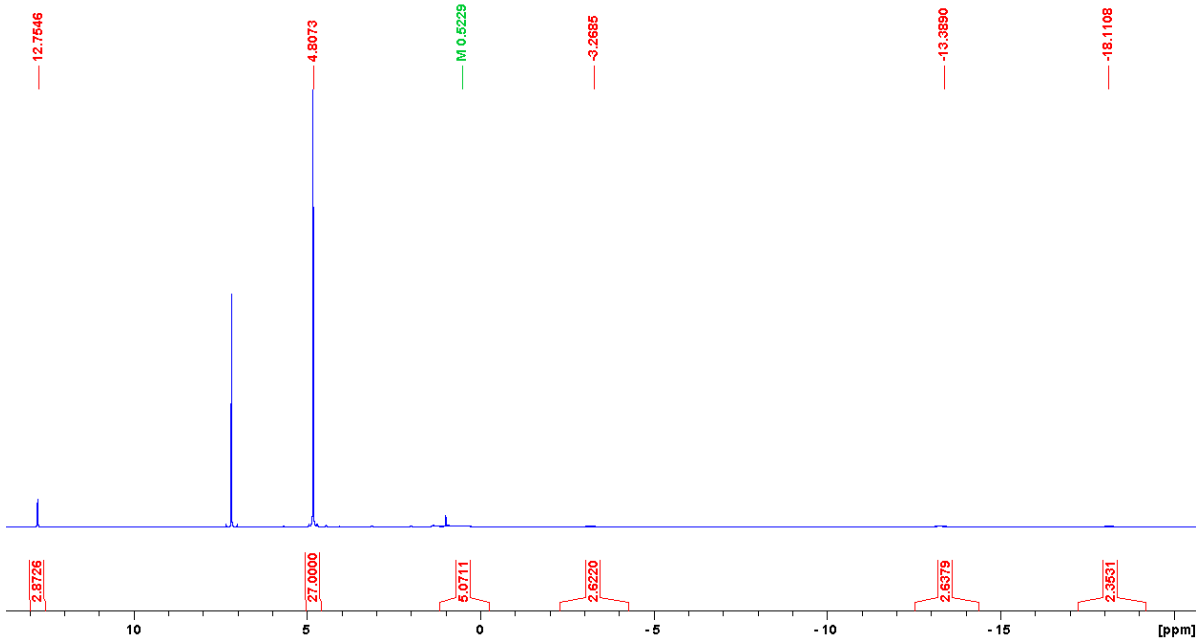

Figure S25. ^{1}H NMR spectrum of **Nd-3** (R = $CF_2CF_2CF_3$, R′ = ^{t}Bu) in C_6D_6.

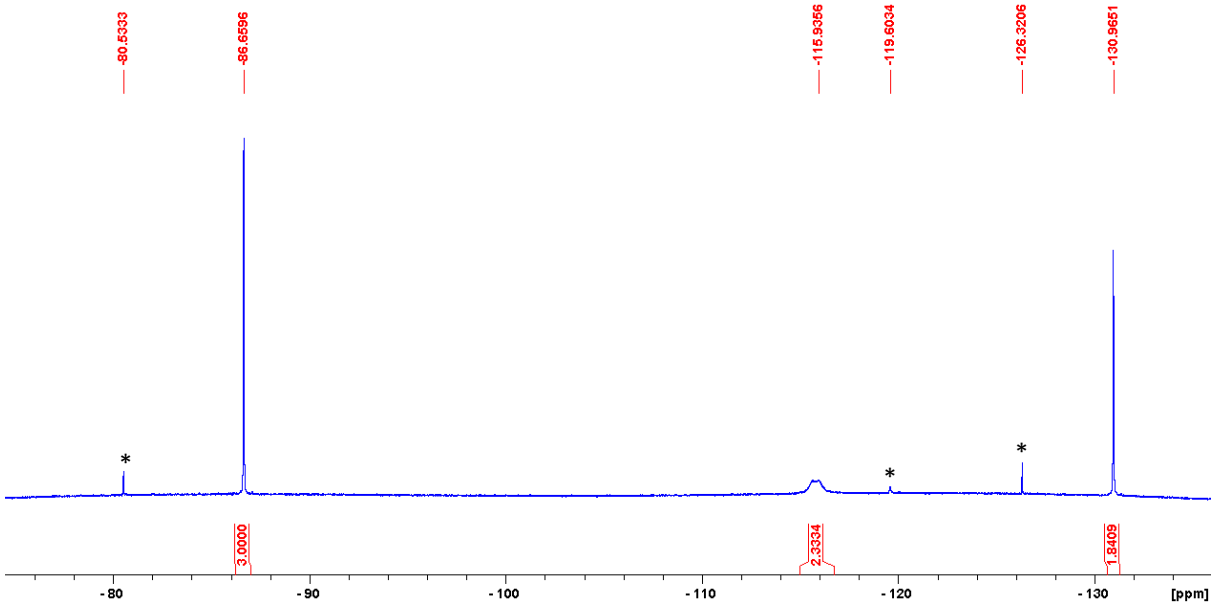

Figure S26. ^{19}F NMR spectrum of **Nd-3** (R = $CF_2CF_2CF_3$, R′ = ^{t}Bu) in C_6D_6. The * symbol indicates resonances assigned to H_3(**3**) ligand.

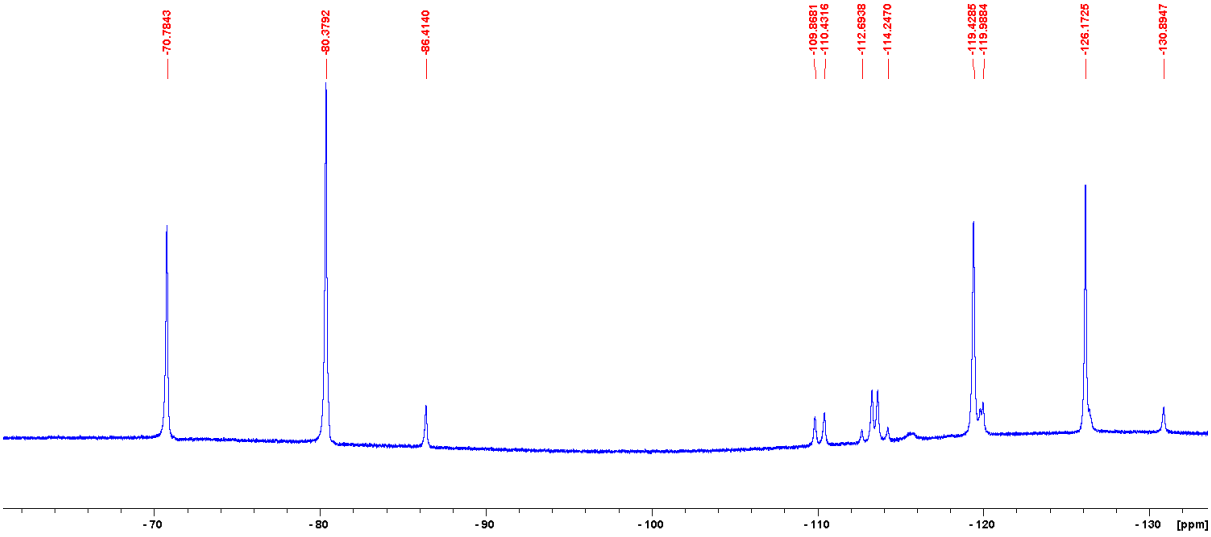

Figure S27. ^{19}F NMR spectrum after stirring a 1:1:1 ratio of $Yb[N(SiMe_3)_2]_3$, $Nd[N(SiMe_3)_2]_3$, and H_3(**3**) in toluene for 1 hour.

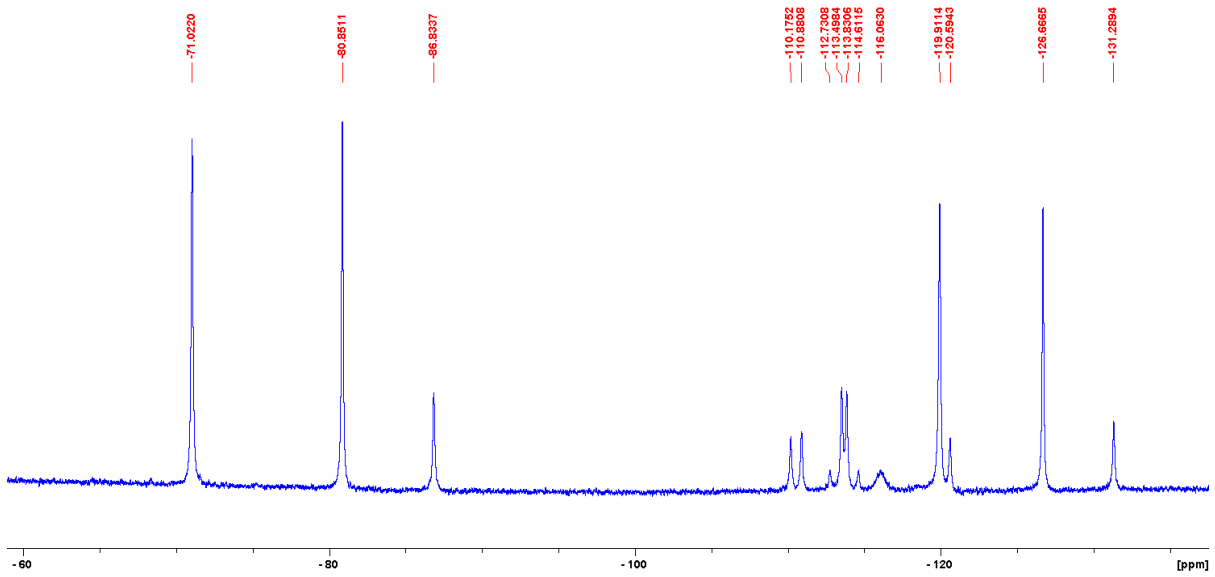

Figure S28. ^{19}F NMR spectrum after stirring a 1:1:1 ratio of $Yb[N(SiMe_3)_2]_3$, $Nd[N(SiMe_3)_2]_3$, and H_3(**3**) in toluene for 24 hours.

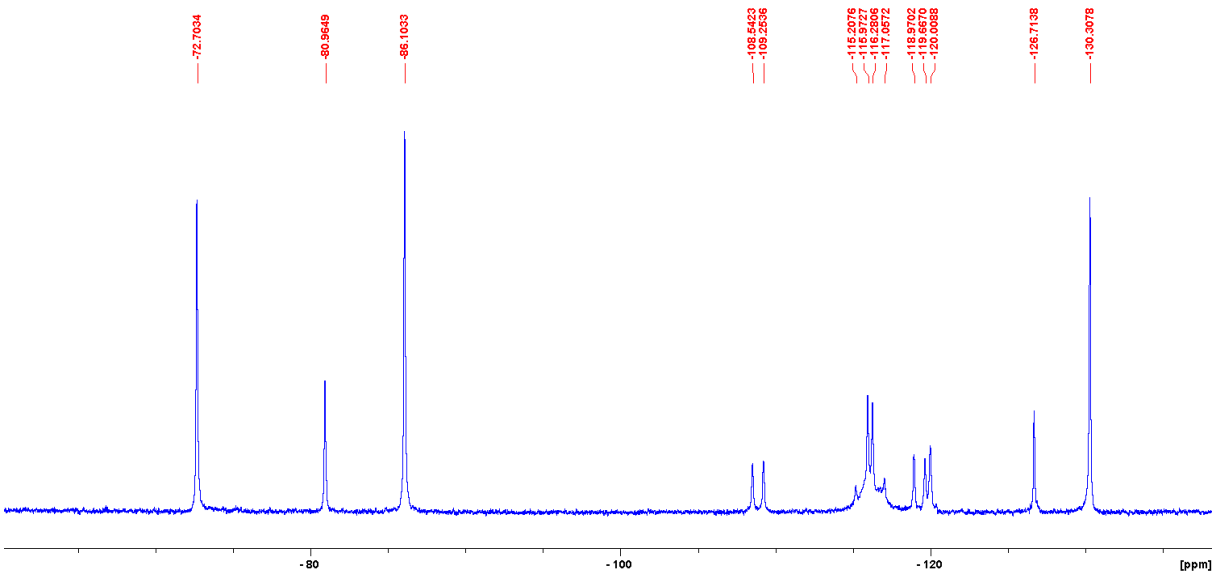

Figure S29. ^{19}F NMR spectrum after refluxing a 1:1:1 ratio of $Yb[N(SiMe_3)_2]_3$, $Nd[N(SiMe_3)_2]_3$, and H_3(**3**) in toluene for 24 hours.

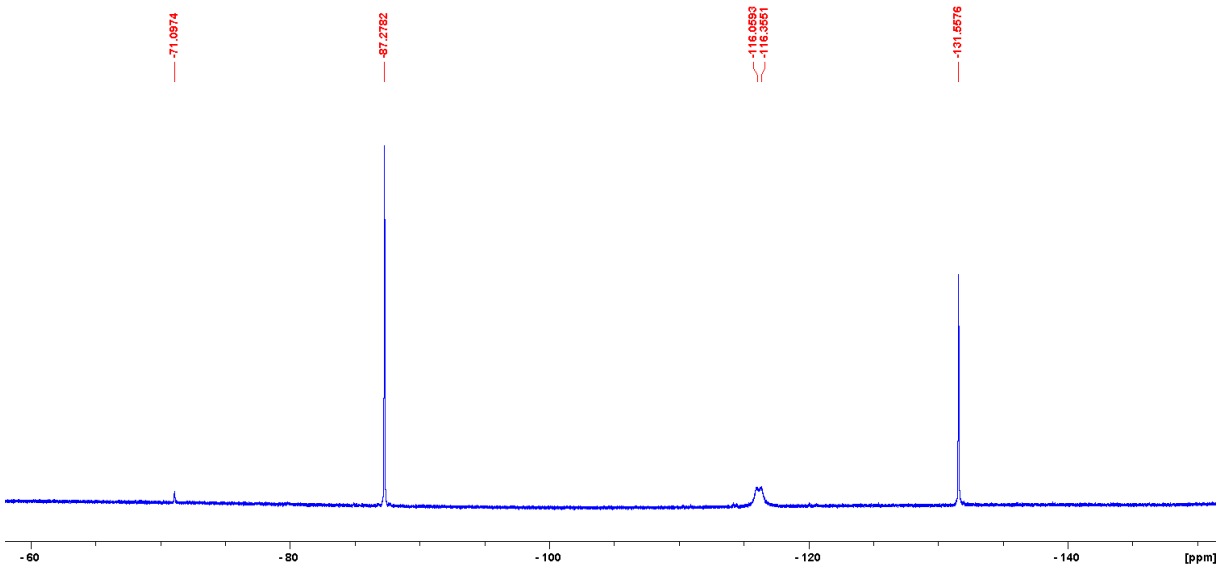

Figure S30. ^{19}F NMR spectrum after stirring a 1:1 ratio of **Nd-3** and $Yb[N(SiMe_3)_2]_3$ in toluene for 24 hrs. The peak at δ -71.1 ppm is assigned to the CF_3 resonance in **Yb-3**.

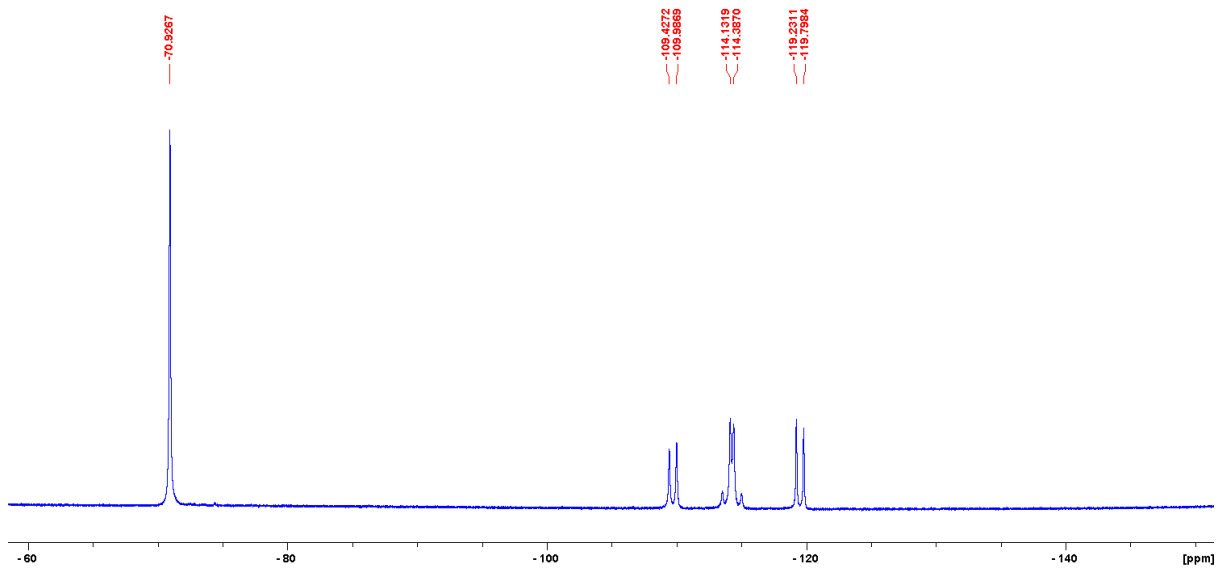

Figure S31. ^{19}F NMR spectrum after stirring a 1:1 ratio of **Yb-3** and $Nd[N(SiMe_3)_2]_3$ in toluene for 24 hrs.

III. IR spectra

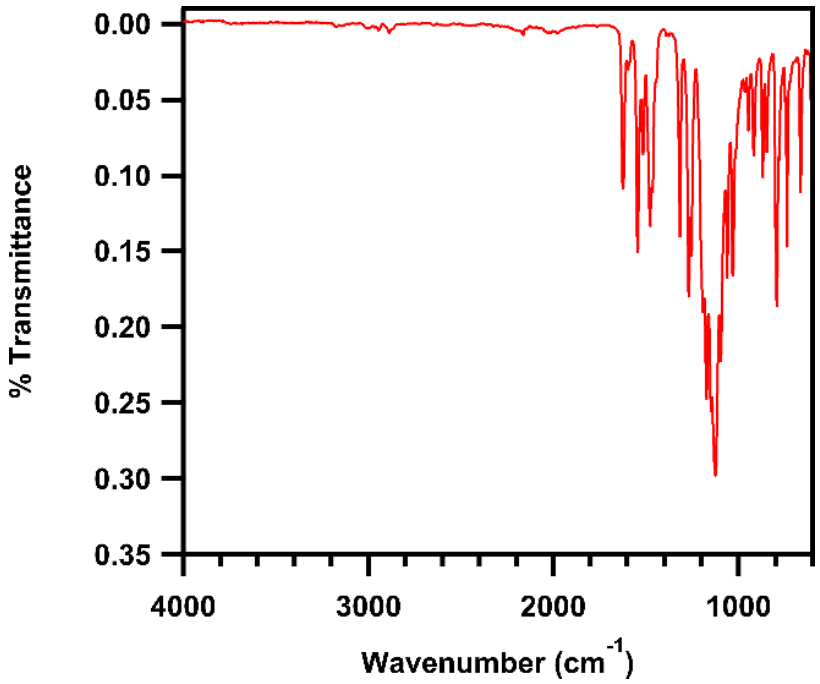

Figure S32. IR spectrum (ATR) of **Yb-1** (R, R′ = CF_3).

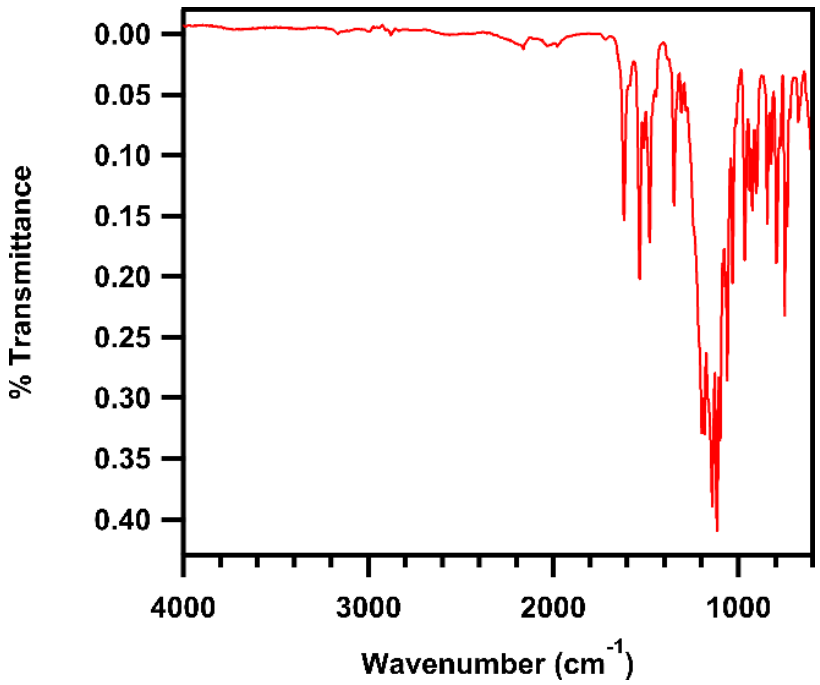

Figure S33. IR spectrum (ATR) of **Yb-2** (R = $CF_2CF_2CF_3$, R′ = CF_3).

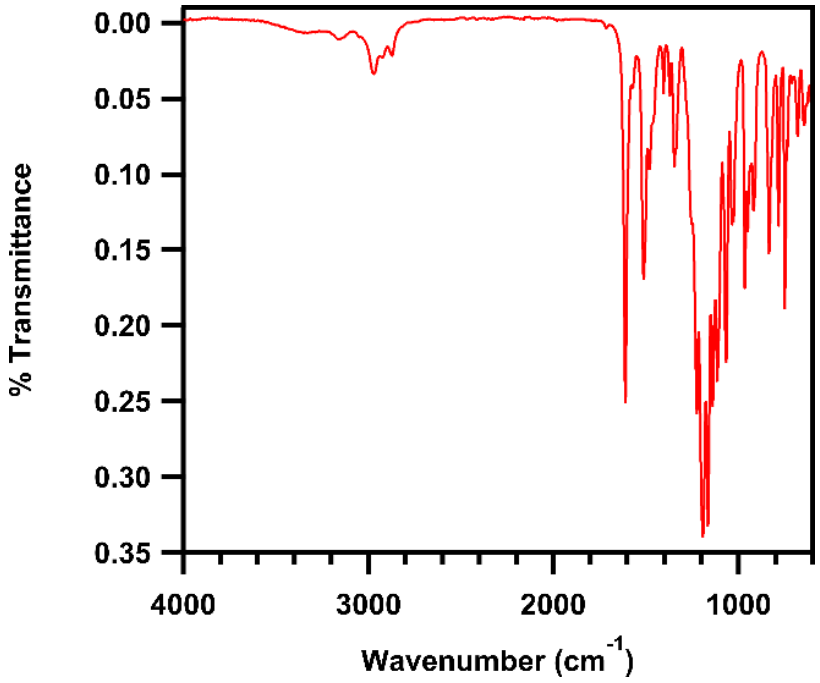

Figure S34. IR spectrum (ATR) of **Yb-3** (R = $CF_2CF_2CF_3$, R′ = ^{t}Bu).

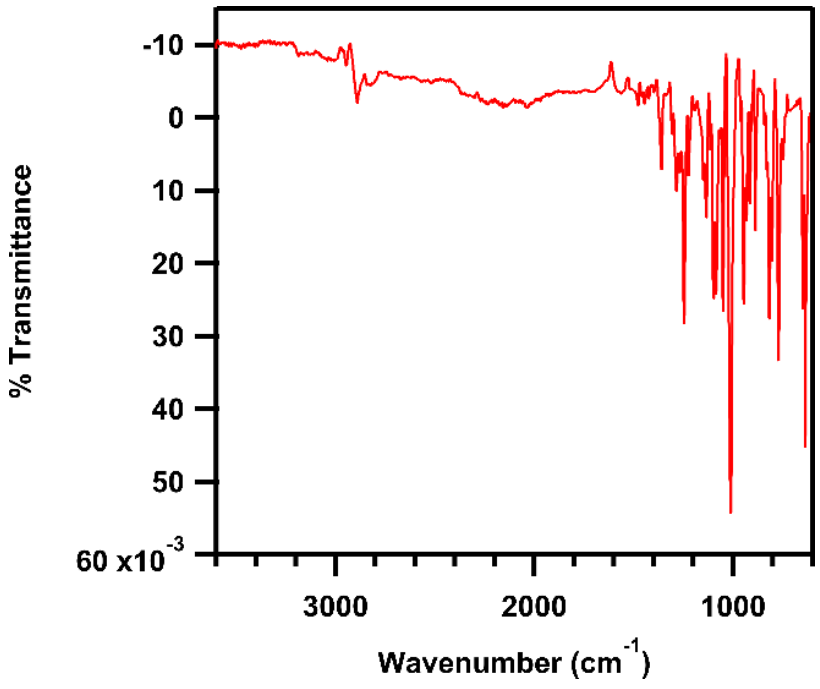

Figure S35. IR spectrum (ATR) of **Yb-4** (R = CF_3, R′ = Me).

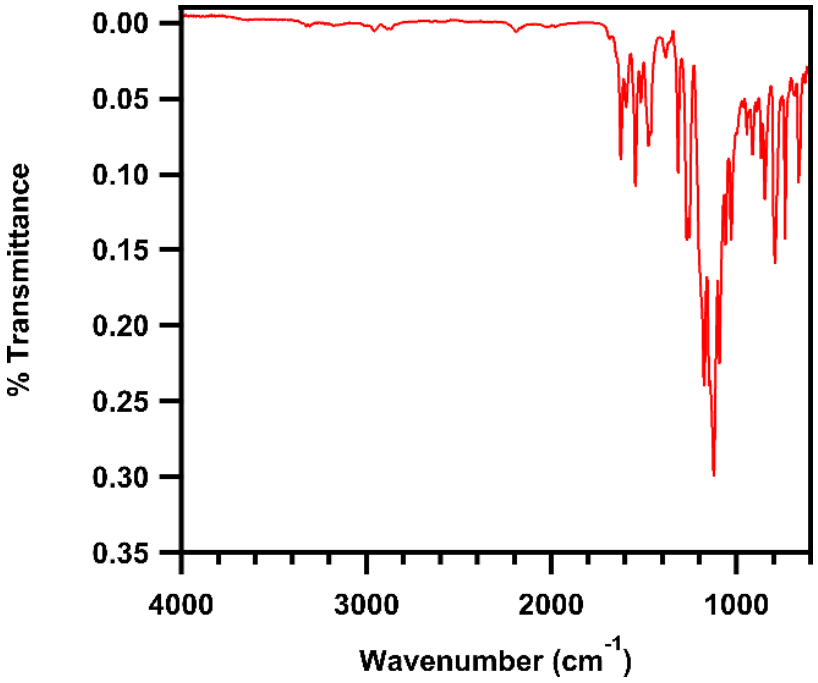

Figure S36. IR spectrum (ATR) of **Er-1** (R, R′ = CF_3).

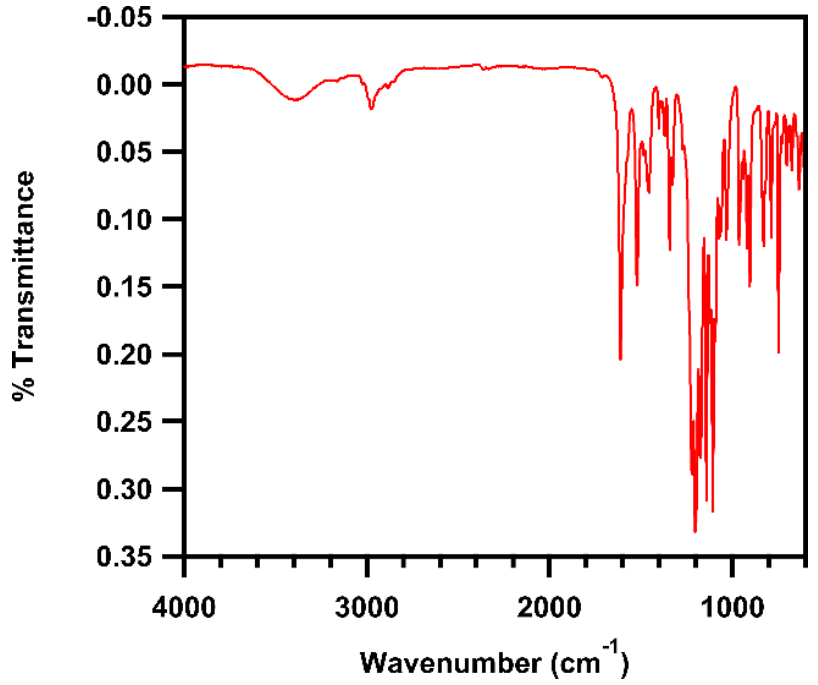

Figure S37. IR spectrum (ATR) of **Nd-3** (R = $CF_2CF_2CF_3$, R′ = ^{t}Bu).

IV. TGA plots

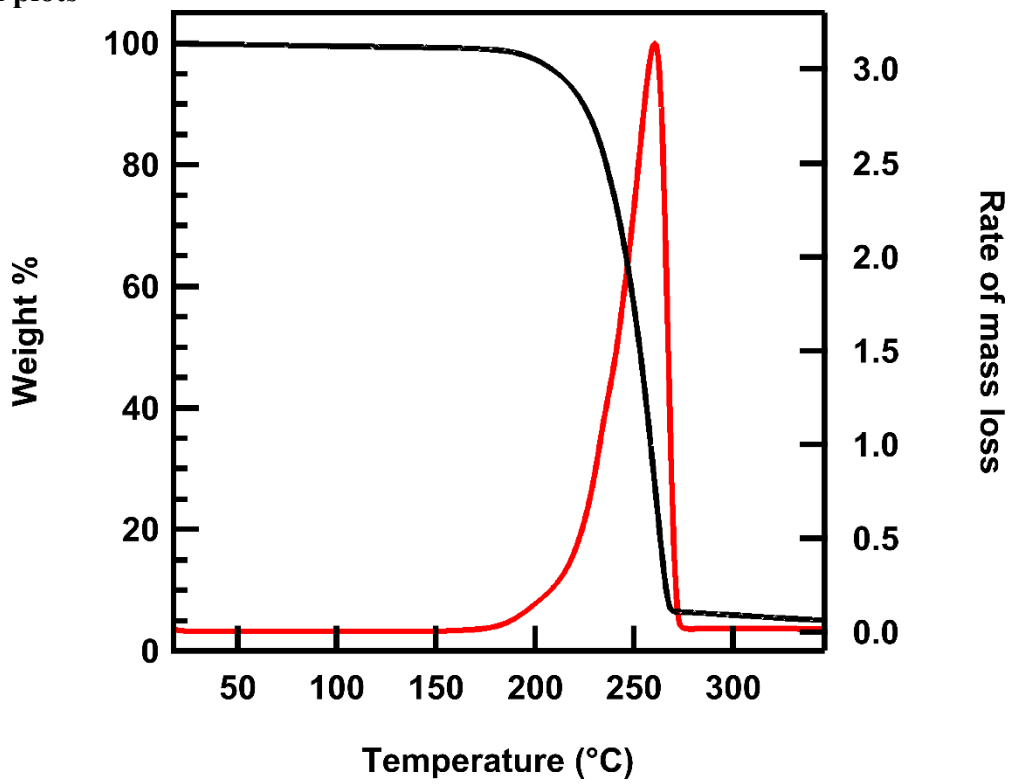

Figure S38. TGA trace of Yb(TRAC). % weight loss over temperature (black), and 1st derivative of mass loss over temperature (red).

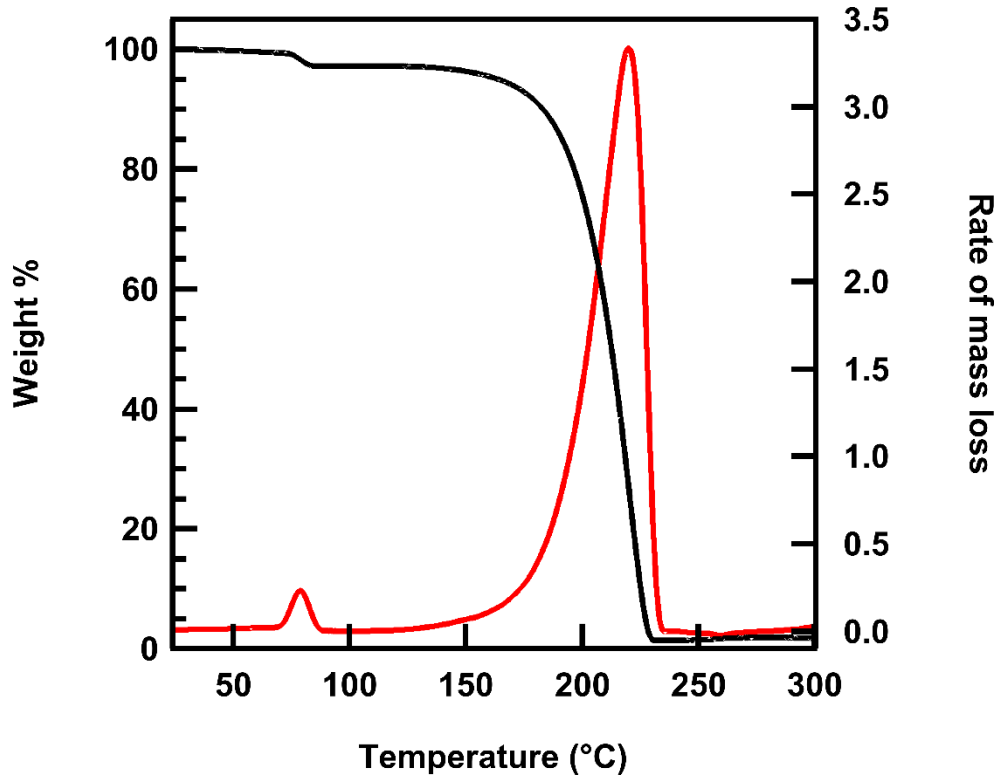

Figure S39. TGA trace of **Yb-1**. % Mass loss over temperature (black), and 1st derivative of mass loss over temperature (red). The small mass loss before 100 °C is attributed to small amounts of water or hydrolysis due to exposing the sample briefly to air during loading.

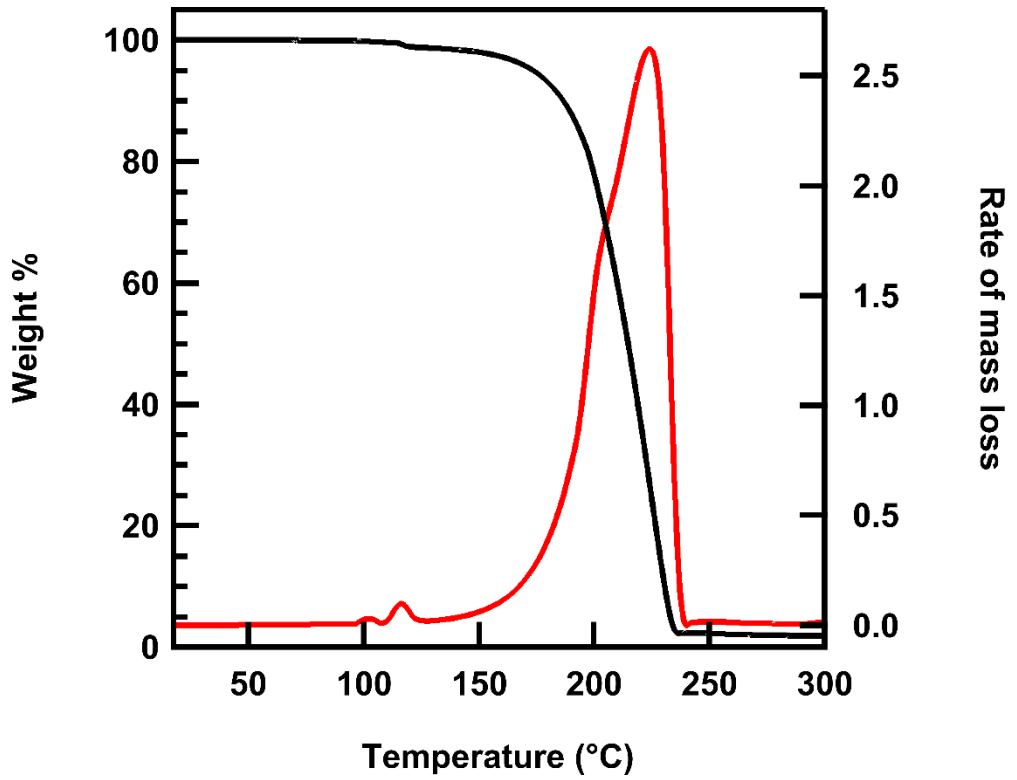

Figure S40. TGA trace of **Yb-2**. % Mass loss over temperature (black), and 1st derivative of mass loss over temperature (red). The small mass loss after 100 °C is attributed to small amounts of water or hydrolysis due to exposing the sample briefly to air during loading.

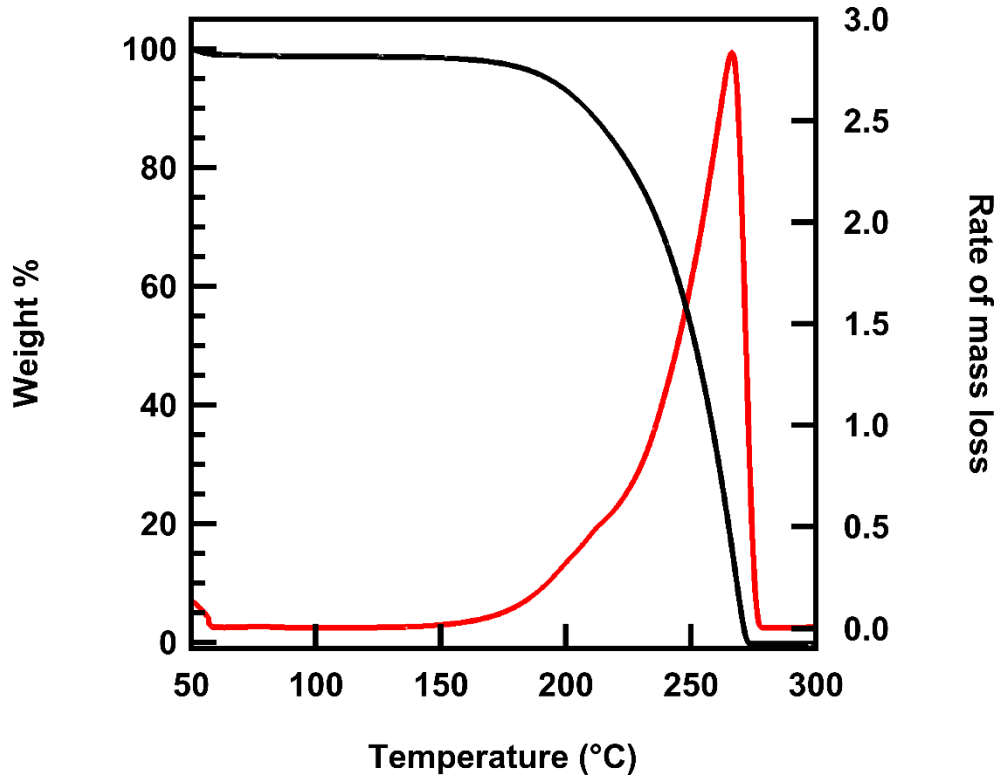

Figure S41. TGA trace of **Yb-3**. % Mass loss over temperature (black), and 1st derivative of mass loss over temperature (red). The small mass loss after 50 °C is attributed to desolvation of co-crystallized Et_2O or pentane.

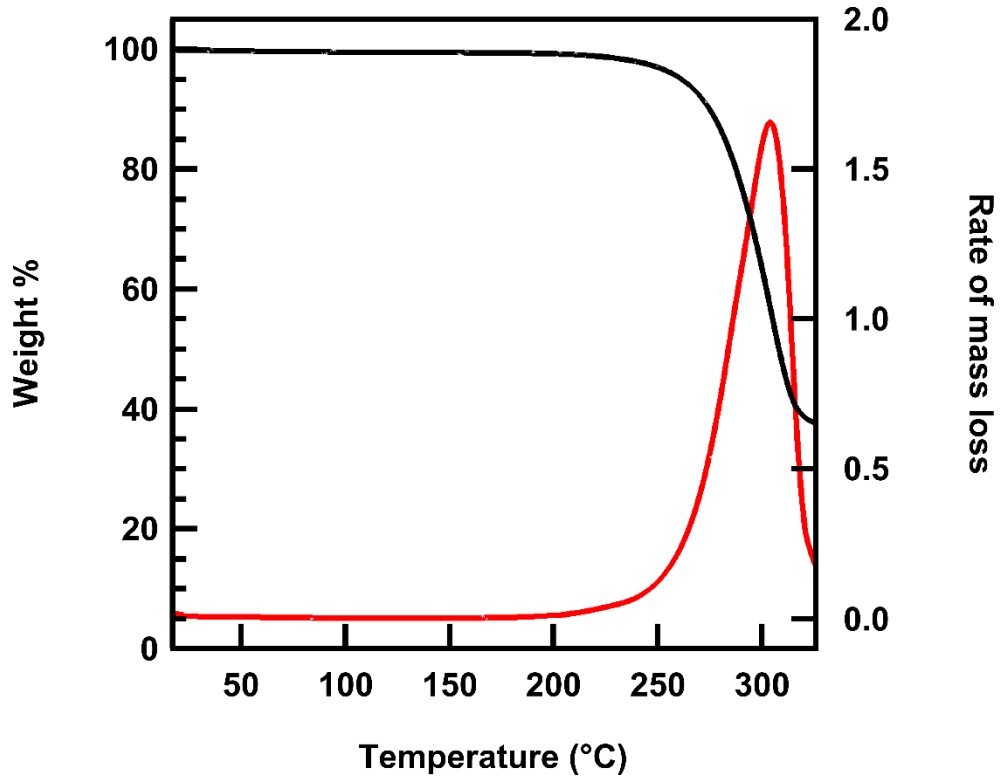

Figure S42. TGA trace of **Yb-4**. % Mass loss over temperature (black), and 1st derivative of mass loss over temperature (red).

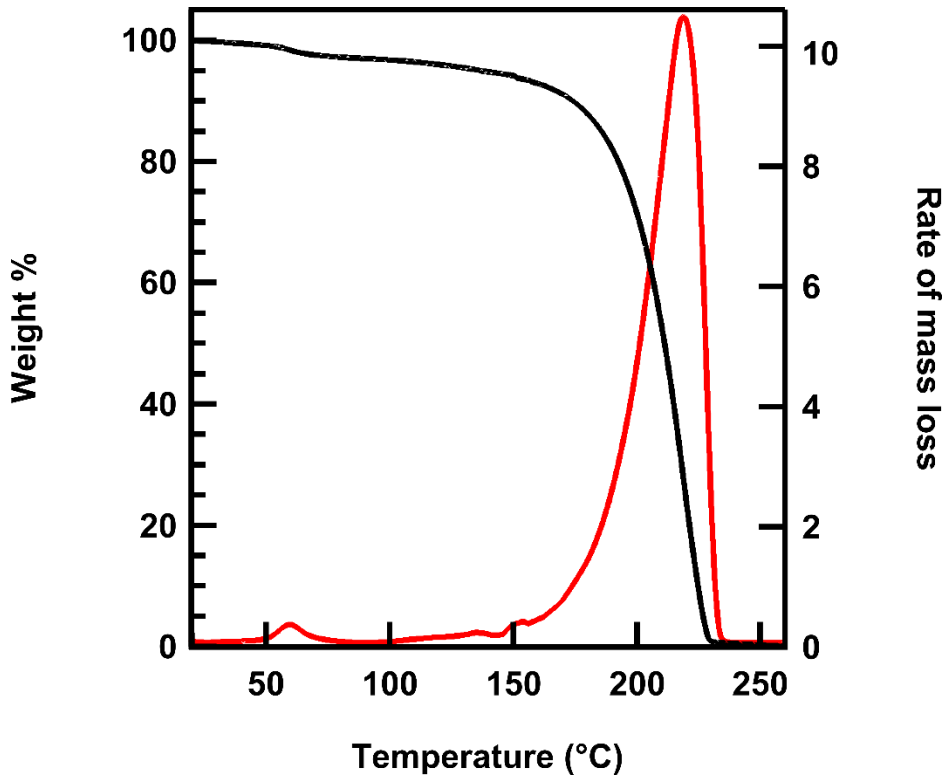

Figure S43. TGA trace of **Er-1**. % Mass loss over temperature (black), and 1st derivative of mass loss over temperature (red). The small mass loss after 50 °C is attributed to small amounts of water or hydrolysis due to exposing the sample briefly to air during loading, as observed for **Yb-1**.

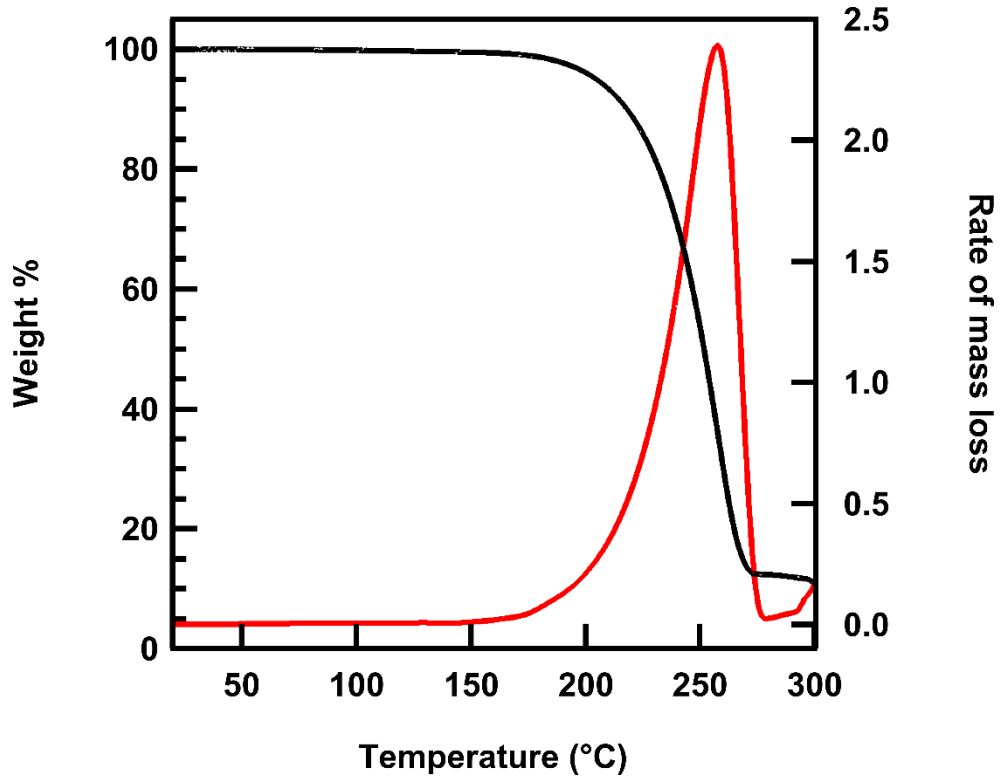

Figure S44. TGA trace of **Nd-3**. % Mass loss over temperature (black), and 1st derivative of mass loss over temperature (red).

V. DFT calculations

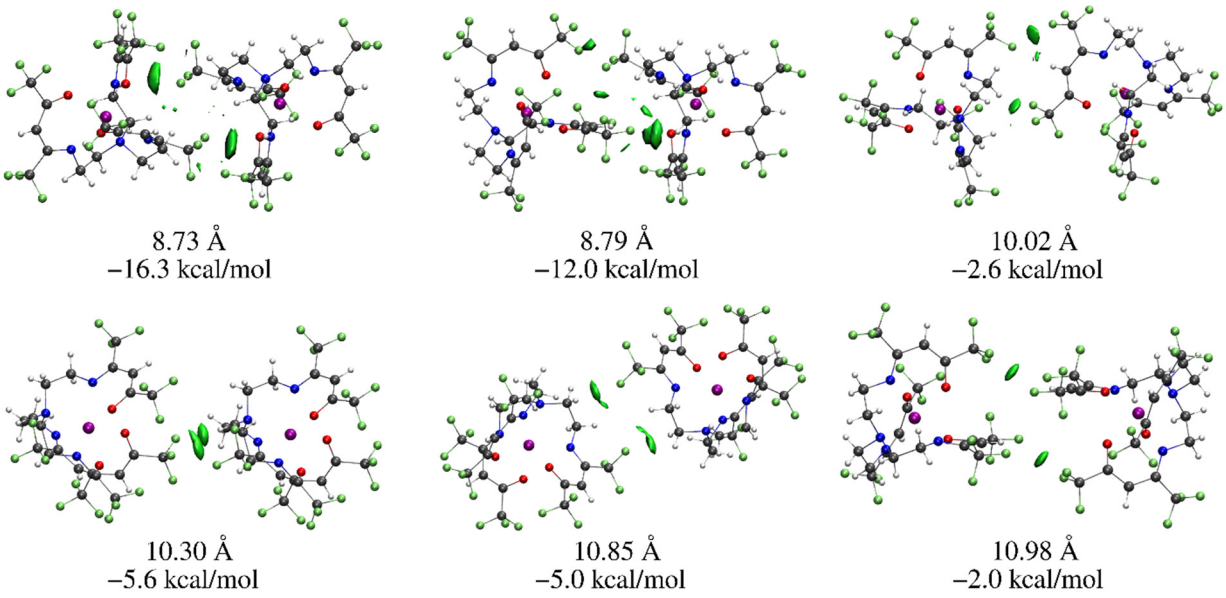

Figure S45. Interacting pairs in **Yb-1**. Green isosurfaces represent stabilizing non-covalent interactions. Each pair is labeled by its Yb-Yb distance in Å and its interaction energy in kcal/mol.

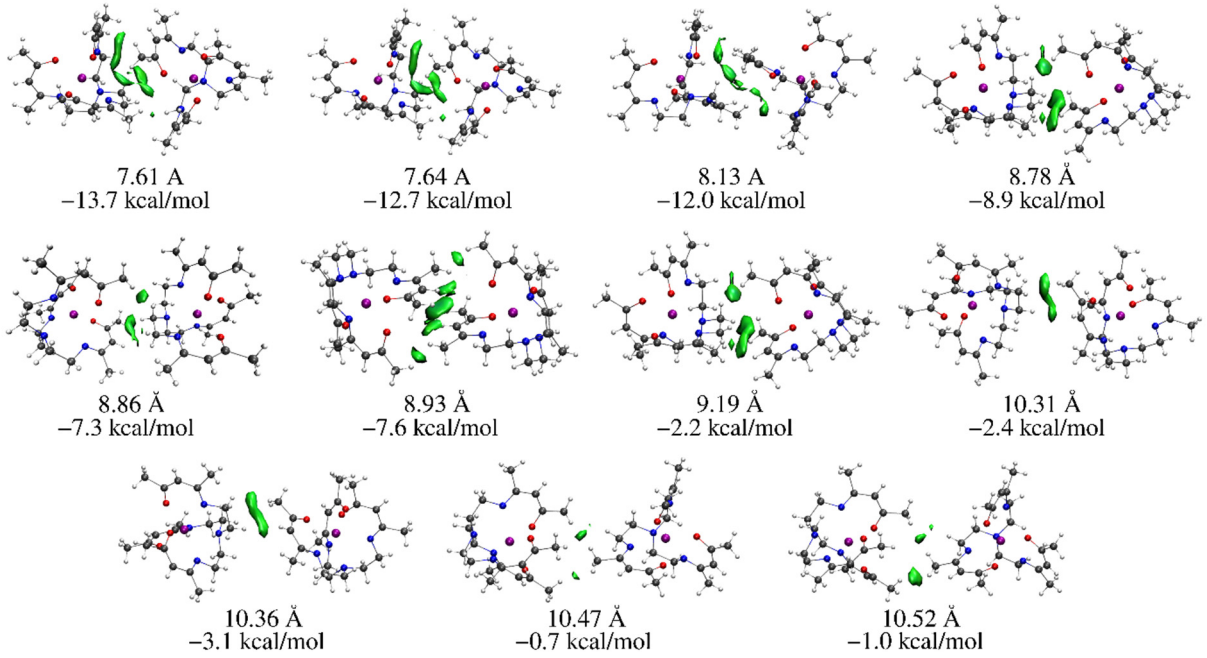

Figure S46. Interacting pairs in Yb(TRAC). Green isosurfaces represent stabilizing non-covalent interactions. Each pair is labeled by its Yb-Yb distance in Å and its interaction energy in kcal/mol.

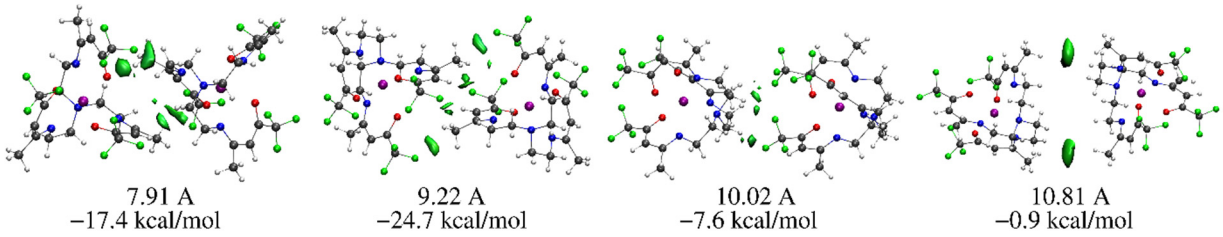

Figure S47. Interacting pairs in **Yb-4**. Green isosurfaces represent stabilizing non-covalent interactions. Each pair is labeled by its Yb-Yb distance in Å and its interaction energy in kcal/mol.

VI. Sample calculation of twist angle

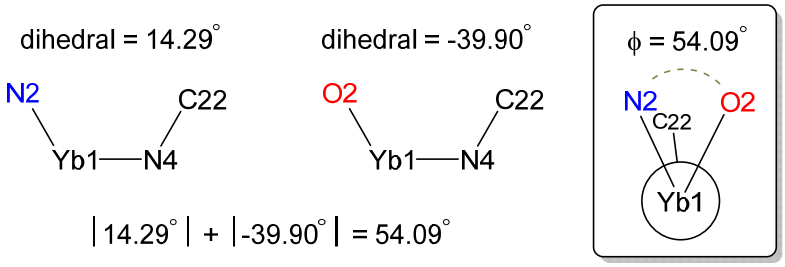

Figure S48. Sample calculation used to determine the twist angles for each complex. The absolute value of the C-N4-Ln-O and C-N4-Ln-N dihedral angles for each β-ketoiminate subunit (where N4 is the capping atom) were summed and the values obtained for each arm averaged to obtain the twist angles and standard deviations provided in Table 1. The values and labeled atoms shown above are from the structure of **Yb-1**.